ELSEVIER

NeuroImage

www.elsevier.com/locate/ynimg
NeuroImage 31 (2006) 1453 – 1474

Three-dimensional locations and boundaries of motor and premotor cortices as defined by functional brain imaging: A meta-analysis

Mary A. Mayka,[a,b] Daniel M. Corcos,[a,b,c,e] Sue E. Leurgans,[e] and David E. Vaillancourt[a,b,d,*]

[a]Department of Movement Sciences, University of Illinois at Chicago, Chicago, IL 60612, USA
[b]Department of Bioengineering, University of Illinois at Chicago, Chicago, IL 60612, USA
[c]Department of Physical Therapy, University of Illinois at Chicago, Chicago, IL 60612, USA
[d]Department of Neurology and Rehabilitation, University of Illinois at Chicago, Chicago, IL 60612, USA
[e]Department of Neurological Sciences, Rush University Medical Center, Chicago, IL 60612, USA

Received 14 July 2005; revised 31 January 2006; accepted 3 February 2006
Available online 29 March 2006

The mesial premotor cortex (pre-supplementary motor area and supplementary motor area proper), lateral premotor cortex (dorsal premotor cortex and ventral premotor cortex), and primary sensorimotor cortex (primary motor cortex and primary somatosensory cortex) have been identified as key cortical areas for sensorimotor function. However, the three-dimensional (3-D) anatomic boundaries between these regions remain unclear. In order to clarify the locations and boundaries for these six sensorimotor regions, we surveyed 126 articles describing pre-supplementary motor area, supplementary motor area proper, dorsal premotor cortex, ventral premotor cortex, primary motor cortex, and primary somatosensory cortex. Using strict inclusion criteria, we recorded the reported normalized stereotaxic coordinates (Talairach and Tournoux or MNI) from each experiment. We then computed the probability distributions describing the likelihood of activation, and characterized the shape, extent, and area of each sensorimotor region in 3-D. Additionally, we evaluated the nature of the overlap between the six sensorimotor regions. Using the findings from this meta-analysis, along with suggestions and guidelines of previous researchers, we developed the Human Motor Area Template (HMAT) that can be used for ROI analysis. HMAT is available through e-mail from the corresponding author.

Keywords: Supplementary motor area; Primary motor cortex; Premotor cortex; Regions of interest; Sensorimotor

Introduction

In neuroimaging research, there are two general techniques often used to analyze functional neuroimaging data. One approach combines group data from multiple subjects (Worsley et al., 1996; Lazar et al., 2002), producing a task-related group activation map in stereotaxic space. This method gives us the ability to identify activation foci that are common between subjects during a specific task. Another method used to analyze neuroimaging data is a region of interest (ROI) analysis. This technique provides an important method for quantifying the volume and intensity of activation in specific brain regions (Friston, 1997). In order for both techniques to deliver precise and accurate results, it is critical to be able to clearly and consistently locate and identify the location and boundaries for each functional ROI.

Currently, there is consensus that different functions exist for the cortical premotor and sensorimotor regions underlying motor control. These regions can be sectioned into three main divisions: the mesial premotor cortex (MPMC), the lateral premotor cortex (LPMC), and the sensorimotor cortex (SMC) (Roland and Zilles, 1996; Rizzolatti et al., 1998; Luppino and Rizzolatti, 2000). MPMC and LPMC corresponds to Brodmann's area 6, whereas SMC is divided into the primary motor cortex (M1) (Brodmann's area 4), and the primary somatosensory cortices (S1) (Brodmann's areas 1, 2, and 3). The functional distinction between motor and somatosensory areas has long been recognized, and there is agreement that the subregions of area 6 subserve distinct functions (Woolsey et al., 1952; Barbas and Pandya, 1987; Picard and Strick, 1996; Rizzolatti and Luppino, 2001; Schubotz and von Cramon, 2003). For instance, MPMC can be divided rostrally and caudally using the ventral anterior commissure (VCA) line into the pre-supplementary motor area (pre-SMA) and supplementary motor area proper (SMA proper), respectively (Rizzolatti et al., 1998; Picard and Strick, 2001). Additionally, LPMC can be subdivided along the rostral and caudal plane (PMr and PMc) (Barbas and Pandya, 1987; Matelli et al., 1991), and also along the dorsal and ventral plane (PMd and PMv) (He et al., 1993; Fink et al., 1997).

* Corresponding author. Department of Movement Sciences (M/C 994), University of Illinois at Chicago, 808 South Wood Street, 690 CME, Chicago, IL 60612, USA. Fax: +1 312 355 2305.
E-mail address: court1@uic.edu (D.E. Vaillancourt).
Available online on ScienceDirect (www.sciencedirect.com).

1053-8119/$ - see front matter © 2006 Elsevier Inc. All rights reserved.
doi:10.1016/j.neuroimage.2006.02.004

Studies such as these have advanced our understanding of the location and boundaries of the premotor and sensorimotor ROIs. However, it has been recommended that a probabilistic model be used when characterizing the location of an activated voxel (Fox et al., 1998; Amunts et al., 2000; Rademacher et al., 2001a) due in part to the inherent variability involved in functional neuroimaging data. For instance, variability is introduced during steps such as post-processing, filtering, motion correction, and normalization. Additionally, several studies have shown that the general morphology and cytoarchitecture of the brain is variable between subjects and exhibits a probabilistic nature (Amunts et al., 1999; Chiavaras et al., 2001; Grefkes et al., 2001; Rademacher et al., 2001b). To further complicate matters, it is known that functional boundaries do not necessarily correspond to either macro or microanatomical structures, which can lead to a structure–function mismatch (Rademacher et al., 1993).

Accordingly, while there are anatomical and physiological data in humans supporting functional distinctions for each of the six motor and premotor brain ROIs, their three-dimensional boundaries and locations in a standardized coordinate space remain unclear. Therefore, the purpose of this meta-analysis was three-fold: (1) to determine the locations and extent of six sensorimotor ROIs based on the data available in the neuroimaging literature, (2) to estimate boundaries between selected ROIs in stereotaxic space, and (3) to create an ROI template in stereotaxic space. First, in order to determine the location and extent of each motor ROI, we reviewed 126 articles that had used a motor task and reported activation foci from any combination of the six cortical motor ROIs. The ROIs included MPMC (pre-SMA and SMA), LPMC (PMd and PMv) and SMC (M1 and S1). Because it has been recommended that a probabilistic model be used when characterizing the location of an activated voxel (Fox et al., 1998; Amunts et al., 2000; Rademacher et al., 2001a), we then used the activation likelihood estimation (ALE) method developed by Turkeltaub et al. (2002) to localize the distributions of the activation foci in stereotaxic space. This technique is based on the assumption that a single coordinate represents a probability distribution, which allows us to determine the likelihood that at least one activation focus lies within any given voxel. Second, to estimate boundaries we characterized the limit of one region in relation to an adjacent region. Third, based on previously established anatomical criteria in conjunction with the data generated from our probability distributions, we drew the ROIs in Talairach space to create the Human Motor Area Template (HMAT). Our findings for these three-dimensional ROIs are presented in the results section and in the discussion, we compare our estimated boundaries with previous suggestions from the literature.

Methods

The outline of the methods section is as follows. First, we discuss the specific inclusion criteria for the articles and coordinates, the ROI categorization, and the exclusion of outliers. Next, we discuss the data processing steps that include the generation of the activation likelihood estimates, significance testing, and boundary estimates. Lastly, we discuss how we created the ROI template.

Inclusion criteria for articles and coordinates

This review examined spatial coordinate data of healthy individuals performing motor control tasks of the mouth and upper and lower limbs from motor control literature between 1997 and 2003. Articles reporting activations (deactivations were not considered) in the motor, premotor, and primary somatosensory regions of the brain were identified via PubMed. Search criteria included keywords and combinations of keywords such as motor, visuomotor, fMRI, PET, imaging, supplementary motor area, SMA, pre-SMA, premotor cortex, LPMC, PMd, PMv, sensorimotor cortex, primary motor cortex, somatosensory cortex, primary sensory cortex, SMC, M1, or S1. We only included studies that imaged the whole brain (minimally from the top of the brain to the cerebellum) and reported data in the normalized stereotaxic reference systems of either Talairach and Tournoux (1988) or Montreal Neurological Institute (MNI) (Evans et al., 1994). In all, a total of 126 articles were examined (Appendix A).

Coordinates from the articles listed in Appendix A were carefully inspected to ensure that they had been reported using radiological convention: x = right/left (+/−), y = rostral/caudal (+/−) and z = dorsal/ventral (+/−), and transposed if reported otherwise. In the Talairach brain, the center coordinate (0, 0, 0) is the intersection of the VCA with the anterior/posterior commissural plane. Because the MNI brain differs in shape and size from the Talairach brain – specifically, “MNI brains are higher, deeper, and longer with increasing differences further from the center of the brain” (Brett et al., 2002) – any MNI coordinates not reported in Talairach space were converted using the transformation equations for above the AC line ($z \geq 0$): $x' = 0.9900x$, $y' = 0.9688y + 0.0460z$, $z' = -0.0485y + 0.9189z$ (Duncan et al., 2000; http://www.mrc-cbu.cam.ac.uk/Imaging/Common/mnispace.shtml). For the SMC and LPMC regions, coordinates were stripped of laterality distinction. This was done so as to include as many coordinates as possible in the data analysis. The laterality distinction for MPMC was not removed because of its medial location.

Regions of interest categorization

This meta-analysis defines the locations and boundaries of six regions based on data reported in the neuroimaging literature: SMA proper, pre-SMA, PMd, PMv, M1, and S1. Data from each experiment including the *xyz* coordinate of peak activation, name of the region specified by the authors (e.g., anatomical location, functional region, Brodmann area), and a brief overview of the experimental parameters were recorded into a single composite database. Next, based on the label assigned by the authors of the study, information was classified into one of three primary groups: MPMC, LPMC, and SMC. A coordinate was classified based on the typical information reported such as functional label, Brodmann area, anatomical location, and Talairach coordinates. Combinations of the above classifiers were commonly used. For example, we would categorize a coordinate with the labels precentral gyrus and area 6 into the LPMC region. If a coordinate could not be definitively identified, it was excluded from the data set. For example, a coordinate merely labeled precentral gyrus with no other qualifiers does not provide enough information to make a distinction between M1 and LPMC, and therefore it would be excluded. After grouping into the three composite regions,

coordinates were then subdivided into one of the six regions. Again, if a coordinate from the composite group could not be further classified into the individual region, it was excluded from the individual region analysis although it did remain in the composite group. For instance, while a coordinate labeled lateral premotor cortex would be classified into the LPMC region, it could not be further sorted into either the PMd or PMv categories. The specific rules used to define each region are described in the following sections.

Mesial premotor cortex (MPMC)

Data points marked as belonging to mesial Brodmann's area 6 and/or functionally as mesial/medial PMC, supplementary motor area/SMA, pre-supplementary motor area/pre-SMA, and/or described anatomically as being located on the mesial portion of the superior frontal gyrus were grouped into the MPMC region. Coordinates were subsequently categorized as pre-SMA if it had been given a designation of pre-, anterior, or rostral, or SMA proper if it had been given a designation of proper, posterior, or caudal.

Lateral premotor cortex (LPMC)

Data for the lateral premotor cortex region was classified in two steps by first compiling into one composite region, and then into its dorsal or ventral regions. Coordinates that we specifically identified as LPMC included those functionally named premotor cortex, dorsal/dorso-lateral premotor cortex, ventral/ventro-lateral premotor cortex, lateral premotor cortex, Brodmann's area 6 or lateral area 6, and/or anatomically described as being on the rostral or anterior precentral gyrus, caudal or posterior superior/middle/inferior frontal gyrus, or located laterally on the middle frontal gyrus. There was considerable variation in the nomenclature for this region. As a result, coordinates were generally labeled using a combination of the above descriptors. For instance, both Broca's area and PMv have been described as being located in the opercular portion of the inferior frontal gyrus. Therefore, a coordinate labeled opercular inferior frontal gyrus would only have been included in the LPMC category if another qualifying label had been used, such as Brodmann's area 6. Coordinates that were described as being dorsal or superior, and/or located within the dorsal/superior premotor cortex or superior frontal gyrus were further categorized into the PMd region, and those that were described as being inferior or ventral, and/or located within the ventral precentral gyrus or the inferior frontal gyrus were categorized into the PMv region. As specified earlier, coordinates were categorized only if its description was clearly reported.

Sensorimotor cortex (SMC)

Data points were included in the sensorimotor cortex region if they were noted as belonging to Brodmann's area 1, 2, 3, or 4, functionally as SMC, M1, S1, sensory, motor, somatosensory, or anatomically located on or in the central sulcus, postcentral gyrus, paracentral lobule, or caudal or posterior bank of the precentral gyrus. This region was then subdivided into the primary motor area if the point was named Brodmann's area 4, M1, primary motor, paracentral lobule, and/or on the caudal or posterior bank of precentral gyrus. Coordinates were classified into the primary sensory area if named primary sensory area, BA 1, 2, and/or 3, postcentral gyrus, or other comparable variants upon these designations. The regions were subdivided into M1 or S1 if and only if such a distinction was reported.

Exclusion of outliers

Exclusion criteria were implemented to minimize the chance that an individual study reporting incorrect coordinates would influence the boundary estimation. After segregating into different ROIs, coordinates were converted into a functional data set using the 3dUndump command in AFNI (Cox et al., 1995). A coordinate was removed from the data set if its two-dimensional Euclidean distance ($d = ((x_i - x_{peak})^2 + (y_i - y_{peak})^2)^{1/2}$) was greater than 1.5 interquartiles above the upper quartile, which is the usual criterion used to identify outliers on boxplots (Rosner, 2000). Two-dimensional calculations were performed for each plane. These outliers were then visually inspected to verify that they were in the incorrect part of the brain. For instance, a coordinate labeled as SMC that was reported considerably rostral to the VCA line, or a premotor coordinate that was reported well caudal to the VCA line would typically have been excluded from analysis. In all, approximately 4% of the data points were excluded from the analysis.

Data processing

The following sections describe the data processing of the classified coordinate data.

Activation likelihood estimation

Having categorized all the coordinates into their respective ROIs, we then estimated each region's location and spatial distribution using the activation likelihood estimation method (Turkeltaub et al., 2002). Additionally, we quantified the overlapping area between two regions in order to estimate their functional boundary. In neuroimaging studies such as the ones used in this review, the location of a specific focus of activation is reported based on group data obtained from a number of subjects. In addition to the functional variability found between subjects, there is also a certain amount of variability introduced into the data based on a number of technical issues such as imaging technique, post-processing procedures (normalization, co-registration, smoothing, filtering, etc), as well as inter-subject anatomical differences. These complications inherently limit the accuracy and precision of localization. For these reasons, an activation focus is most accurately viewed not as a single point, but as a localization probability distribution centered at a given coordinate. Following the transformation of all the foci into probability distributions, a whole brain map can be created by assigning each voxel a value proportional to the probability that it contains at least one of the points in the data. This value is the activation likelihood estimate (ALE) (Turkeltaub et al., 2002).

A pre-determined field of view (FOV) of the dimensions 111 × 131 × 111mm^3 was sectioned into 2mm^3 voxels. The FOV ranged from $x = -84$ to 46, $y = -60$ to 50, and $z = -24$ to 86, ensuring that any coordinate from the dataset would fall within its boundaries. For each voxel, we calculated the spatial probability for every reported coordinate using a multivariate Gaussian distribution in three dimensions, assuming equal variance in all three directions:

$$p = \frac{e^{-d^2/2\sigma^2}}{(2\pi)^{1.5}\sigma^3},$$

where d is the Euclidean distance between the center of the voxel and the focus, and σ is the standard deviation of the distribution. A σ value of 5mm (FWHM ≈12mm) was selected based on the values for smoothing filters reported in this meta-analysis. The above equation provides the point probability of localization at the center of a given voxel. In order to estimate the probability that a specific focus lies within the entire $2mm^3$ voxel, this value was multiplied by a factor of 8. The probability that any given focus lies within that voxel was determined by taking the union of the probability values for all data points. This gives us an estimate of the likelihood that at least one activation focus will be found in that voxel. By designating a probability value for each voxel in space, an ALE map was created for all voxels within the FOV (Turkeltaub et al., 2002).

Significance testing

In order to determine a threshold for significance, the ALE values for each ROI were compared to those obtained from randomly distributed sets of foci, matched in size. For illustrative purposes, Fig. 1A shows the histograms of the ALE values for the SMC map (blue), and its corresponding noise maps (red). One thousand sets of randomly distributed coordinates were created within the FOV and processed identically to the literature specified coordinates. The relative frequencies of fixed bins for ALE values were obtained for reach random data set, and then averaged to obtain a single histogram representing the ALE noise distribution. This histogram was used as a null hypothesis distribution to analyze the significance of ALE values within a specific ROI using the omnibus single threshold test (Holmes et al., 1996; Nichols and Holmes, 2002). This statistical test obtains P values for a statistical map against permutations of null hypothesis maps by ranking the maximal voxel value in the statistical map against the maximal voxel values obtained from the null hypothesis simulations. For every ROI dataset, the maximal ALE value in the statistical map derived from the literature was greater than the maximal values of its corresponding 1000 null hypothesis simulation values.

To identify the particular voxels within the statistical map for which the null hypothesis could be rejected, the probability of obtaining ALE values greater than a given threshold under the null hypothesis was calculated as the fraction of the total voxels in the noise histogram greater than that threshold. Thus, the ALE value corresponding to a chosen α for the statistical test was the value with 100*α% of the area under the noise histogram to its right. The null hypothesis (random distribution of foci) was rejected for any voxel within the statistical map for which ALE values were greater than the α threshold. A conservative α value of 0.0001 was selected to reduce type I error (Turkeltaub et al., 2002). The threshold for SMC corresponded to an ALE value of 0.0136 (Fig. 1A).

Boundary estimation

We used the ALE maps to estimate the boundaries of the individual ROIs. For each ROI, all significant data were ranked by ALE value and converted into percentiles. The probability of obtaining a particular ALE value was calculated by determining the area under the ALE histogram to the right of that value (Fig. 1B). Voxels that were found within the center of an ROI are the most likely to be activated (e.g., a high ALE value). Due to the fact that there are few highly significant voxels in any given region, there exists a low probability of locating a voxel in an ROI containing a high ALE value. Conversely, the voxels found on the outer edges of a region are less likely to be strongly activated than those in the center (e.g., a low ALE value), and there is a high probability of locating a voxel with a low ALE value in an ROI. When viewed as a map in three-dimensional space, these probabilities describe the spatial distribution of a region. It is important to note that this method of assigning a percentage based on the ALE value does not affect the spatial location of the region. Rather, the patterns that arise reflect the distribution of the data.

Since we were interested in the extent and boundaries of a region as a whole as opposed to its somatotopy, we included articles across multiple effectors (e.g., arm, leg, hand, see Appendix A). In this meta-analysis, 115 articles included movements related to the fingers, hands, or arms. There were 11 articles that looked at foot or leg effectors. There were 14 articles that looked at oral effectors. Because some of our regions are

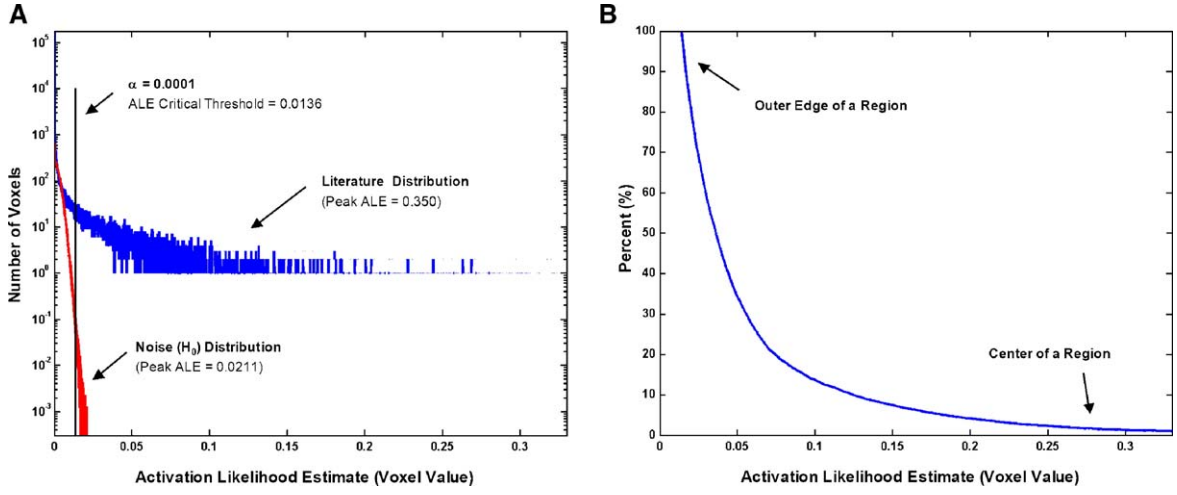

Fig. 1. (A) Histograms of the activation likelihood estimate (ALE) voxel values within the brain for SMC (blue), and the averaged histograms of the randomly generated noise maps (red). The omnibus critical ALE threshold was determined by setting the fraction of voxels in the random (null hypothesis) histogram greater than the critical threshold (α=0.0001). (B) Percentile curve generated from the original ALE values. These are the percentiles used in subsequent figures.

somatotopically organized such as SMC or SMA proper, portions of these ROIs may be under-estimated.

When we had data from two adjacent regions, we estimated their boundary by calculating the degree of overlap between the two. In order to evaluate this overlapping area we took the absolute value of the differences of the percentage maps and created a difference map. A line of equal probability can be found at the points where there is no difference in percentage values between the two regions. This line provides an estimate of the boundary where there is an equal likelihood of being in one region versus the other. The resulting difference map is a U-shaped function in two-dimensional space, where on either side of the line we find a graded distribution. This information provides a quantification of the level of confidence we have that a specific data point falls within one particular region as opposed to its adjacent region. Where data were not available for two adjacent regions, we estimated this boundary by describing a region's probabilistic extent. Although we were not able to quantitatively describe these boundaries to the same degree, this information does provide us with an estimate of its location.

Human motor area template (HMAT)

After compiling and analyzing all the reported coordinates for each region, the Human Motor Area Template (HMAT) was drawn based on the boundary information ascertained from this analysis in conjunction with the anatomical landmarks that have been previously outlined. Regions were drawn using boundary information from this analysis when there existed an overlap between two adjacent regions. For these regions, the line of equal probability was used as the boundary line. The six boundaries that were estimated using overlap data from this analysis included the caudal limit of pre-SMA where it overlapped with the rostral limit of SMA proper, the dorsal limit of PMv where it overlapped with the ventral limit of PMd, the rostral limit of S1 where it overlapped with the caudal limit of M1, the rostral limit of SMC where it overlapped with the caudal limit of LPMC, the rostral limit of SMC where it overlapped with the caudal limit of MPMC, and the lateral limit of MPMC where it overlapped with the medial limit of LPMC. For boundaries occurring where there was no overlap data for two adjacent regions, the boundary was determined using both the estimates from the probability analysis and suggestions from the literature. These boundaries included the ventral limit of MPMC (the cingulate sulcus), the rostral limit of LPMC (the pre-central sulcus), the caudal limit of S1 (the postcentral gyrus), and the ventral limits of LPMC and SMC (the Sylvian Fissure). As there are no concrete anatomical landmarks delineating the rostral limit of MPMC, this boundary was set using estimates from this probability analysis and suggestions from the literature describing its location in Talairach space (Roland and Zilles, 1996, Fig. 1); (Johansen-Berg et al., 2004, Fig. 1).

Anatomical landmarks were identified using the brains of 15 subjects. Each brain was registered in Talairach space and then averaged together to form a single averaged anatomical structure. Both individual and averaged brains were used for the identification of anatomical landmarks. In drawing the regions, our goal was to ensure that the defined areas encompassed the majority of the reported coordinates while also maintaining proper anatomical boundaries.

Results

The summary statistics for the three composite regions and the 6 individual regions are listed in Table 1. There were 94 articles reporting MPMC, 92 articles reporting LPMC, and 101 articles reporting SMC. Another observation from Table 1 is that researchers do not always specify individual regions, but in many cases will only specify a composite region. The composite regions include both the coordinates segregated into individual regions and the coordinates specified as a composite region. We found that 54% of MPMC coordinates, 57% of LPMC coordinates, and 23% of SMC coordinates were reported as a composite region without distinction between individual subdivisions (e.g., PMd vs. lateral premotor cortex). Thus, researchers were more likely to make a distinction between M1 and S1 than between PMd and PMv or between SMA proper and pre-SMA.

Mesial premotor cortex (MPMC)

For all statistically significant thresholded ALE values, MPMC ranges from $x = -18$ to 16, $y = -32$ to 27, and $z = 33$ to 73 (Table 1). MPMC is located rostral to SMC and medial to LPMC. The probability distribution profile for the composite MPMC region is shown in Fig. 2 (green). Table 1 shows that the peak x, y, and z coordinates for MPMC are $x = -2$, $y = -1$, and $z = 54$. In Table 2A, a detailed presentation of the peaks and ranges for the x and y coordinates in 5mm axial slices is shown. Table 2A also provides the number of coordinates per slice and the area determined by the ALE analysis. The peak coordinates for MPMC indicate that it is located caudal in the dorsal slices (at $z = 70$, $x = -4$ and $y = -8$), and rostral in the ventral slices (at $z = 35$, $x = 1$ and $y = 14$) (Table 2A; Fig. 2). Also, Fig. 2 and Table 2A indicate that the spatial distribution does not shift in the x direction.

Table 1
Overall summary statistics

	N	No. of Studies	Peak$_x$	Peak$_y$	Peak$_z$	Range$_x$	Range$_y$	Range$_z$
MPMC	330	94	−2	−1	54	−18 to 16	−32 to 27	33 to 73
pre-SMA	93	22	−3	6	53	−18 to 16	−7 to 27	33 to 72
SMA proper	60	20	−2	−7	55	−17 to 14	−30 to 7	42 to 76
LPMC	495	92	−26	−6	56	−70 to −9	−21 to 20	−2 to 73
PMd	118	31	−30	−4	58	−55 to −8	−21 to 12	27 to 76
PMv	94	29	−50	5	22	−70 to −31	−8 to 8	−2 to 46
SMC	517	101	−39	−21	54	−69 to 4	−45 to 6	18 to 78
M1	278	68	−37	−21	58	−70 to 4	−43 to 7	19 to 76
S1	119	40	−40	−24	50	−70 to −20	−44 to −9	19 to 72

The table describes the number of coordinates and the number of articles used for each data set. For each region determined by the 95th percentile of the ALE maps, the location of the maximum ALE value (Peak$_x$, Peak$_y$, Peak$_z$), and the extent of ALE map in each plane (Range$_x$, Range$_y$, Range$_z$).

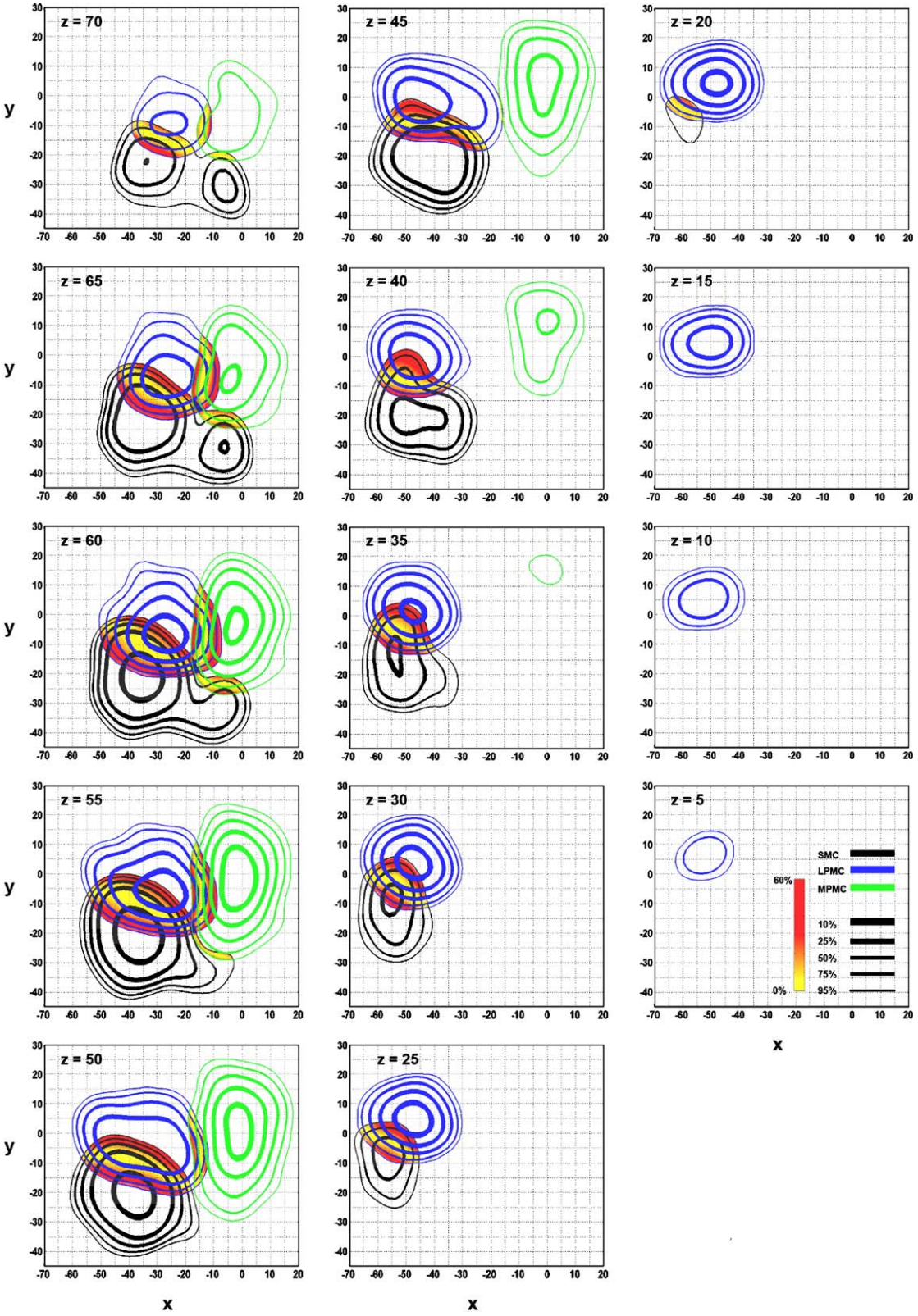

Fig. 2. Color-coded spatial probability maps identify overlap between MPMC (green), LPMC (blue), and SMC (black). Contour lines represent the 95th, 75th, 50th, 25th, and 10th percent probability that the likelihood that an activation focus will fall within the area encompassed by the contour line. Each line thickness corresponds to a specific percentile. The spatial overlap between two regions was quantified as a difference map with no difference in probabilities equal to 0% (yellow regions). An increasing difference in the probability difference maps is shown as a gradation from yellow to red. Areas containing activation from all three regions are purple. Axial slices are shown.

Table 2

z	N	Peak$_x$	Peak$_y$	Range$_x$	Range$_y$
A. Summary statistics for MPMC					
70	0	−4	−8	−16 to 13	−22 to 12
65	4	−4	−8	−18 to 16	−25 to 17
60	22	−3	−5	−18 to 17	−27 to 21
55	45	−2	−2	−18 to 17	−29 to 24
50	82	−2	0	−20 to 17	−30 to 25
45	105	−2	6	−18 to 17	−27 to 26
40	47	0	11	−16 to 13	−27 to 26
35	23	1	14	−6 to 5	10 to 20
B. Summary statistics for pre-SMA					
70	1	−4	6	−9 to 3	0 to 11
65	3	−4	6	−13 to 8	−3 to 17
60	4	−2	6	−15 to 14	−6 to 22
55	17	−2	8	−17 to 16	−7 to 25
50	32	−3	6	−18 to 16	−7 to 27
45	23	−2	8	−17 to 15	−5 to 27
40	11	−2	10	−16 to 13	0 to 25
35	2	2	14	−11 to 9	0 to 22
C. Summary statistics for SMA proper					
75	3	0	−12	−4 to 3	−15 to 0
70	6	−2	−12	−12 to 10	−22 to 0
65	9	−4	−10	−14 to 14	−25 to 2
60	19	−4	−8	−16 to 13	−26 to 7
55	18	−2	−7	−17 to 12	−29 to 7
50	4	−2	−8	−15 to 9	−30 to 6
45	1	−2	−8	−10 to 5	−28 to 2

Summary statistics for MPMC, pre-SMA, and SMA proper. Axially every 5 mm, the location of the peak xy coordinate, and the extent (Range$_x$, Range$_y$) at the 95th percentile of the ALE map is shown. N is the number of raw data coordinates per 5mm axial slice (e.g., z=66 to 70).

There are several important observations regarding the overlap between MPMC and the other two composite areas. First, MPMC crosses into the medial pole of SMC with only a small degree of overlap between MPMC and SMC (Table 3). As shown in Fig. 2, the MPMC/SMC overlap is most noticeable between z = 65 and z = 60. The overlap extends from x = −18 to 2, y = −28 to −17, and z = 52 to 71 for all data within the two regions that is statistically significant, and the peak 3-D coordinates are x = −10, y = −22, and z = 61 (see Table 3). The line of equal probability (Fig. 2, yellow area) between MPMC and SMC is angled in the rostro-lateral to caudo-medial direction. Second, there is considerable overlap between MPMC and LPMC which extends from x = −18 to −7, y = −20 to 12, and z = 45 to 73, with the peak of the overlap at x = −14, y = −6, and z = 59 (Table 3). The line of equal probability between MPMC and LPMC is parallel to midline at approximately x = −15 (Fig. 2). Lastly, a small overlapping region that contains all three composite regions is centered at x = −16, y = −17, z = 61 (Fig. 2, purple).

pre-SMA vs. SMA proper

For all statistically significant thresholded ALE values, pre-SMA ranges from x = −18 to 16, y = −7 to 27, and z = 33 to 72. Table 1 shows that the peak 3-D coordinates for pre-SMA are x = −3, y = 6 and z = 53 and the probability distribution profile is shown in Fig. 3 (blue). Table 2B shows the peaks and ranges of x and y per axial slice from z = 70 through z = 35. Fig. 3 indicates that in the dorsal slices, pre-SMA is caudal and slightly to the left than in the ventral slices. This shift in position can also be observed in Table 2B, where at z = 70, the peak of x is −4 and the peak of y is 6, and at z = 35 the peak of x is 2 and the peak of y is 14.

SMA proper is located caudal and dorsal to pre-SMA (Fig. 3, black). From the statistically significant ALE values, SMA proper ranges from x = −17 to 14, y = −30 to 7, z = 42 to 76. Table 1 shows that the peak 3-D coordinates were x = −2, y = −7 and z = 55. Table 2C shows more detail regarding the peaks and ranges of x and y per axial slice from z = 75 through z = 45. As shown in Fig. 3, SMA proper appears to shift slightly rostral and left in the ventral slices. Table 2C also reflects this trend, where at z = 75 the peak of x is 0 and the peak of y is −12, and at z = 45 the peak of x is −2 and the peak of y is −8.

The overlapping region between the pre-SMA and SMA proper ranges from x = −14 to 14, y = −7 to 7 and z = 43 to 69 (Table 3). The line of equal probability (yellow area in Fig. 3) between pre-SMA and SMA proper traverses through the y = 0 line (corresponding to the VCA), even across different z slices.

Lateral premotor cortex (LPMC)

For all statistically significant ALE values, LPMC ranges from x = −70 to −9, y = −21 to 20, and z = −2 to 73. The peak 3-D coordinates were x = −26, y = −6 and z = 56 (Table 1), and it is located just rostral to SMC (Fig. 2). Table 4A shows the peaks and ranges of x and y per axial slice from z = 75 through z = 0. Fig. 2 and the peak x and y values in Table 4A indicate that LPMC gradually moves in a rostro-lateral direction. For instance, Table 4A shows that at z = 75 the peak of x is −22 and the peak of y is −12, and at z = 20 the peak of x is −48 and the peak of y is 4.

Fig. 2 shows the overlap between LPMC and SMC. This overlap ranges from x = −68 to −14, y = −23 to 6, and z = 17 to 76 (Table 3). The line of equal probability (Fig. 2, yellow area) between SMC and LPMC is angled in the rostro-lateral to caudo-medial direction throughout the entirety of the overlap.

Table 3
Overlapping regions

	Peak$_x$	Peak$_y$	Peak$_z$	Range$_x$	Range$_y$	Range$_z$
MPMC and LPMC	−14	−6	59	−18 to −7	−20 to 12	45 to 73
MPMC and SMC	−10	−22	61	−18 to 2	−28 to −17	52 to 71
LPMC and SMC	−41	−9	48	−68 to −14	−23 to 6	17 to 76
MPMC, LPMC and SMC	−16	−17	61	−13 to −19	−20 to −15	51 to 68
SMA proper and pre-SMA	−1	0	55	−14 to 14	−7 to 7	43 to 69
PMd and PMv	−45	−2	37	−57 to −34	−11 to 8	30 to 46
M1 and S1	−41	−22	49	−65 to −20	−37 to −9	21 to 71

Characteristics of the overlapping regions as determined by the difference maps. The Table describes the location of the maximal overlap (Peak$_x$, Peak$_y$, Peak$_z$) and the location of the extent of the overlap (Range$_x$, Range$_y$, Range$_z$).

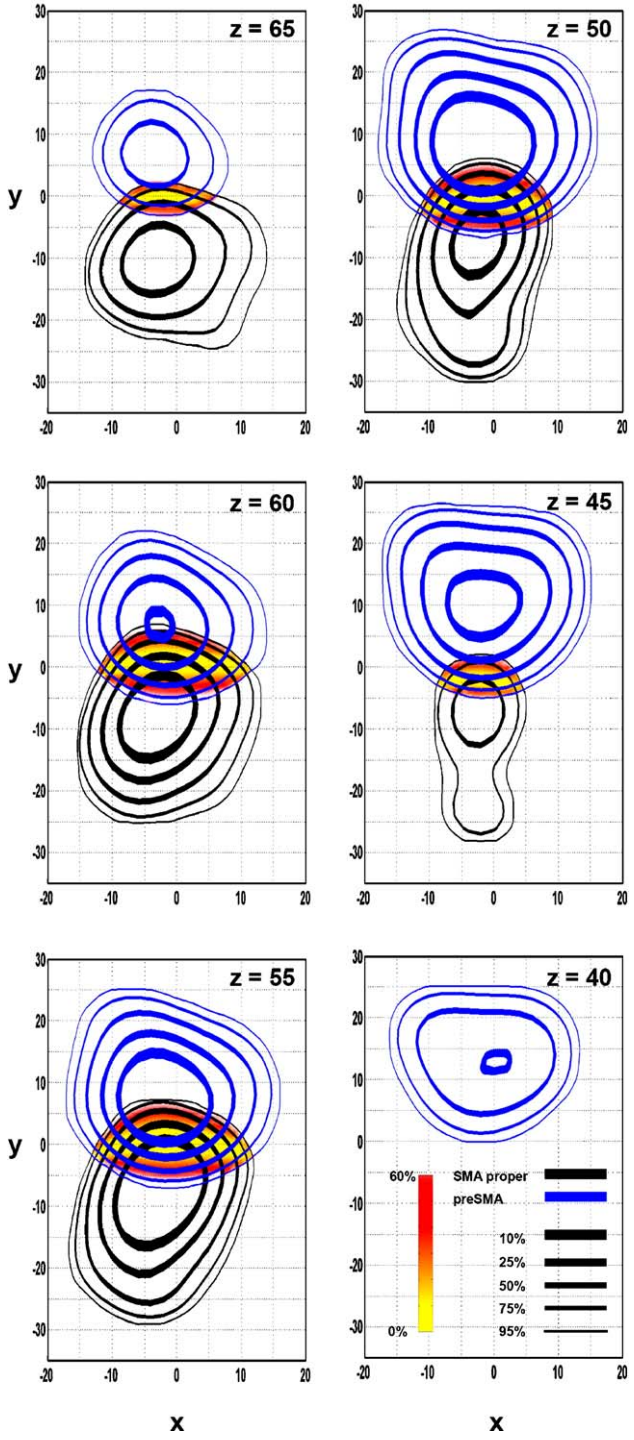

Fig. 3. Contour lines and spatial probability maps between the regions designated as SMA proper (black) and pre-SMA (blue). Contour lines and difference maps are identical to that described in Fig. 2. Axial slices are shown.

PMd vs. PMv

Table 1 indicates that the peak 3-D coordinates for PMd are $x = -30$, $y = -4$, and $z = 58$. For all statistically significant ALE values, PMd ranges from $x = -55$ to -8, $y = -21$ to 12, and $z = 27$ to 76. The probability distribution profile for PMd is shown in the coronal plane in Fig. 4 (black). Table 4B shows the peaks and ranges of x and y per axial slice from $z = 70$ through $z = 30$. The overall distribution of PMd moves in a rostro-lateral direction, with the greatest shift in the lateral dimension (Fig. 4). For instance, at $z = 70$ the peak of x is -30 and the peak of y is -10, and at $z = 30$ the peak of x is -44 and the peak of y is -2 (Table 4B).

For all statistically significant ALE values, PMv ranges from $x = -70$ to -31, $y = -8$ to 8, and $z = -2$ to 46. The probability distribution profile for PMv is shown in Fig. 4 (blue), and Table 1 indicates that the peak 3-D coordinates were $x = -50$, $y = 5$ and $z = 22$. Table 4C shows the peaks and ranges of x and y per axial slice from $z = 45$ through $z = 0$. The overall distribution of PMv is rostral to PMd and the position of PMv along the vertical axis remained fairly constant in the more ventral slices (Fig. 4). For instance, at $z = 40$ the peak of x is -54 and the peak of y is 2, and at $z = 0$ the peak of x is -52 and the peak of y is 6 (Table 4C).

The overlap between PMd and PMv ranges from $x = -57$ to -34, $y = -11$ to 8, and $z = 30$ to 46 (Table 3). The line of equal

Table 4

z	N	Peak$_x$	Peak$_y$	Range$_x$	Range$_y$
A. Summary statistics for LPMC					
75	0	−22	−12	−24 to −20	−14 to −11
70	6	−26	−10	−39 to −11	−21 to 7
65	20	−26	−8	−44 to −8	−22 to 15
60	63	−26	−8	−51 to −7	−21 to 18
55	57	−26	−6	−57 to −9	−21 to 17
50	81	−26	−6	−60 to −12	−21 to 16
45	37	−42	−2	−62 to −15	−19 to 15
40	22	−46	0	−64 to −27	−14 to 16
35	35	−48	2	−65 to −30	−13 to 18
30	38	−48	4	−66 to −30	−12 to 20
25	38	−48	4	−67 to −30	−10 to 20
20	48	−48	4	−68 to −31	−9 to 19
15	23	−48	4	−68 to −35	−7 to 17
10	14	−50	4	−67 to −38	−5 to 16
5	10	−52	6	−63 to −42	−2 to 15
0	3	−52	6	−53 to −48	5 to 10
B. Summary statistics for PMd					
70	1	−30	−10	−38 to 0	−34 to 5
65	7	−30	−8	−43 to 1	−35 to 14
60	31	−30	−6	−49 to −8	−21 to 17
55	22	−30	−4	−53 to −11	−19 to 16
50	30	−28	−4	−54 to −13	−20 to 14
45	11	−40	−2	−55 to −17	−19 to 9
40	6	−42	−2	−56 to −30	−12 to 8
35	8	−42	−2	−55 to −34	−11 to 7
30	2	−44	−2	−52 to −38	−8 to 5
C. Summary statistics for PMv					
45	1	−52	−2	−58 to −46	−6 to 5
40	4	−54	2	−64 to −35	−10 to 14
35	10	−52	2	−66 to −31	−12 to 17
30	18	−48	4	−67 to −31	−12 to 18
25	14	−48	4	−68 to −32	−10 to 18
20	20	−50	5	−69 to −34	−8 to 18
15	11	−50	6	−70 to −37	−7 to 17
10	8	−54	4	−69 to −41	−5 to 17
5	5	−54	6	−64 to −42	−3 to 15
0	3	−52	6	−57 to −45	1 to 13

Summary statistics for LPMC, PMd, and PMv. Axially every 5 mm, the location of the peak xy coordinate, and the extent (Range$_x$, Range$_y$) at the 95th percentile of the ALE map is shown. N is the number of raw data coordinates per 5mm axial slice (e.g., z=66 to 70).

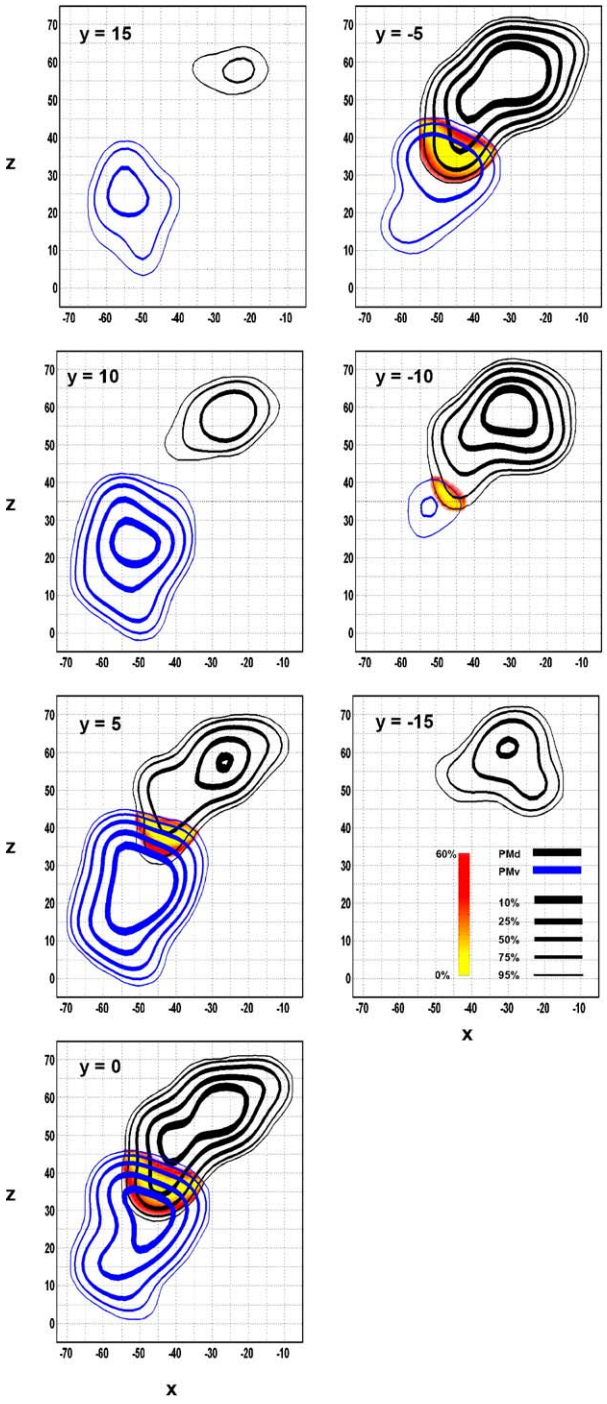

Fig. 4. Contour lines and spatial probability maps between the regions designated as PMd (black) and PMv (blue). Contour lines and difference maps are identical to that described in Fig. 2. Coronal slices are shown.

probability between PMd and PMv is angled in a dorso-lateral to ventro-medial direction (Fig. 4).

Sensorimotor cortex (SMC)

Table 1 shows that the peak 3-D coordinates for SMC are $x = -39$, $y = -21$, and $z = 54$. The probability distribution profile for the composite SMC region is shown in Fig. 2 (black). Based on the statistically significant ALE values, the distribution for SMC ranges from $x = -69$ to 4, $y = -45$ to 6, and $z = 18$ to 78. Table 5A shows the peaks and ranges of x and y per axial slice from $z = 70$ through $z = 20$. From the dorsal-most aspects of the brain through $z \cong 60$, the composite SMC region exhibits a bimodal distribution, with the more medial center at $x = -7$ and $y = -32$, and the more lateral center at $x = -36$ and $y = -23$ (Fig. 2). The medial pole of SMC begins to disappear between $z = 60$ and 55. Fig. 2 also indicates that the overall distribution of SMC gradually moves in a rostral and lateral direction. Table 5A confirms this rostro-lateral shift in that at $z = 70$, the peak of x is -34 and the peak of y is -22, and at $z = 20$ the peak of x is -56 and the peak of y is -8.

M1 vs. S1

For all statistically significant thresholded ALE values, M1 ranges from $x = -70$ to 4, $y = -43$ to 7, and $z = 19$ to 76. The peak 3-D coordinates for M1 (Table 1) were $x = -37$, $y = -21$ and $z = 58$, and the probability distribution profile for M1 is shown in Fig. 5 (black). Table 5B shows the peaks and ranges of x and y per axial

Table 5

z	N	Peak$_x$	Peak$_y$	Range$_x$	Range$_y$
A. Summary statistics for SMC					
70	0	−34	−22	−47 to 3	−42 to −8
65	11	−34	−22	−52 to 4	−44 to −3
60	40	−36	−22	−54 to 3	−44 to 0
55	90	−35	−19	−58 to −1	−43 to 0
50	106	−39	−21	−61 to −14	−42 to 0
45	93	−38	−20	−64 to −20	−40 to 0
40	60	−40	−20	−65 to −24	−37 to 3
35	32	−50	−20	−66 to −30	−33 to 5
30	25	−54	−8	−67 to −39	−30 to 5
25	29	−56	−8	−69 to −44	−26 to 4
20	17	−56	−8	−67 to −51	−19 to 2
B. Summary statistics for M1					
75	0	−8	−26	−39 to −2	−35 to −16
70	6	−34	−22	−46 to 3	−41 to −8
65	29	−34	−22	−49 to 4	−43 to −3
60	59	−36	−21	−53 to 4	−43 to 0
55	70	−37	−21	−56 to −1	−40 to 0
50	37	−36	−20	−58 to −14	−36 to −1
45	24	−38	−18	−59 to −19	−33 to −1
40	12	−40	−18	−61 to −24	−28 to 3
35	8	−54	−8	−64 to −40	−27 to 5
30	17	−56	−6	−67 to −44	−21 to 7
25	8	−56	−6	−70 to −46	−17 to 5
20	8	−56	−6	−68 to −52	−12 to 2
C. Summary statistics for S1					
70	0	−34	−36	−41 to −26	−41 to −25
65	3	−32	−30	−46 to −23	−44 to −21
60	5	−34	−28	−50 to −21	−44 to −15
55	8	−40	−24	−57 to −20	−44 to −10
50	8	−40	−24	−63 to −22	−44 to −9
45	27	−40	−24	−65 to −25	−41 to −10
40	24	−40	−24	−67 to −29	−38 to −10
35	17	−50	−24	−68 to −34	−35 to −9
30	10	−54	−24	−69 to −41	−32 to −9
25	8	−56	−20	−69 to −46	−29 to −10
20	6	−56	−20	−62 to −51	−24 to −13

Summary statistics for SMC, M1, and S1. Axially every 5 mm, the location of the peak xy coordinate, and the extent (Range$_x$, Range$_y$) at the 95th percentile of the ALE map is shown. N is the number of raw data coordinates per 5mm axial slice (e.g., z=66 to 70).

slice from $z = 75$ through $z = 20$. From the dorsal-most aspects of the brain through $z = 60$, M1 exhibits a bimodal distribution with the more medial center at $x = -7$ and $y = -32$ and the more lateral center at $x = -35$ and $y = -23$ (Fig. 5). Fig. 5 also shows that the medial pole of M1 begins to disappear between $z = 60$ and $z = 55$. The peak x and y coordinates from the overall distribution of M1 gradually moves in a rostro-lateral direction (Table 5B, Fig. 5).

The probability distribution profile for S1 is shown in Fig. 5 (blue), and the peak 3-D coordinates of this region were $x = -40$, $y = -24$ and $z = 50$ (Table 1). For all statistically significant ALE values, S1 ranges from $x = -70$ to -20, $y = -44$ to -9, and $z = 19$ to 72. Table 5C shows the peaks and ranges of x and y per axial slice from $z = 70$ through $z = 20$. As seen for M1, the overall distribution of S1 gradually moves in a rostro-lateral direction (Fig. 5). At $z = 70$, the peak of x is at -34 and the peak of y is at -36, and at $z = 20$ the peak of x is at -56 and the peak of y is at -20 (Table 5C).

There is considerable amount of overlap between M1 and S1, which ranges from $x = -65$ to -20, $y = -37$ to -9, and $z = 21$ to 71 (Table 3). The largest amount of overlap occurs at $z = 50$ in the axial plane where it is 40mm long in one direction, and 20mm long in the other (Fig. 5). The line of equal probability between the two runs in a caudo-medial to rostro-lateral direction.

Discussion

The purpose of this study was to develop rigorous guidelines for the three-dimensional location and boundaries of six principle cortical ROIs associated with premotor and sensorimotor control in the human: pre-SMA, SMA proper, PMd, PMv, M1, and S1. The study implemented a probability based meta-analysis of individual activation foci from 126 fMRI and PET articles examining motor tasks. The discussion is organized according to the 3 different composite regions: MPMC, LPMC and SMC. For each region, we compare our data as presented in the tables and figures with the boundaries suggested in the literature.

Mesial premotor cortex (MPMC)

There are 5 boundaries of importance for MPMC that will be presented within the context of our results: the boundary between SMA proper and pre-SMA, the rostral limit of MPMC, the caudal limit of MPMC (the boundary between MPMC and SMC), the ventral limit of MPMC (the boundary between MPMC and CMA), and the lateral limits of MPMC (the boundary between MPMC and LPMC).

pre-SMA vs. SMA proper

MPMC is comprised of two functionally distinct units, with pre-SMA situated rostral to SMA proper. These two regions have been previously differentiated in the monkey (Dum and Strick, 1991; Matelli et al., 1991; Matsuzaka et al., 1992). Since then, this demarcation has been supported in humans across studies using cytoarchitectonic data (Vorobiev et al., 1998; Geyer et al., 2000a), PET (Fink et al., 1997), functional MRI (Deiber et al., 1999), diffusion tensor imaging (Lehericy et al., 2004), and diffusion weighted imaging (Johansen-Berg et al., 2004). The boundary between pre-SMA and SMA proper estimated by the ALE method remained consistent at $y = 0$mm throughout the coronal plane (Fig. 3). Since it is generally accepted that the dividing line between pre-SMA and SMA proper is the VCA (Picard and Strick, 1996), it is necessary that the data from this meta-analysis is in agreement with these previously established boundaries. This demonstrates that the ALE method accurately reflects the data used in the analysis.

Rostral limit of MPMC

Generally, the rostral boundary of MPMC is considered unknown as there are no macroanatomical landmarks (Roland and Zilles, 1996; Geyer et al., 2000a). Cytoarchitectonically, the rostral-most limit of MPMC was shown to be between 22 and 28mm rostral to the VCA line in two subjects (Vorobiev et al., 1998, Fig. 1). Functionally, this boundary has also been depicted at $y \cong 16$ (Roland and Zilles, 1996, Fig. 1), $y = 20$ at $z = 50$ and $y \cong 16$ at $z = 65$ (Picard and Strick, 1996, Fig. 4D), and at $y = 30$ (Johansen-Berg et al., 2004, Fig. 1). This boundary was also quantified at 30mm rostral to the VCA line (17.1% of 175mm in rostro-caudal length) during a study investigating finger movements (Deiber et al., 1999). Based on 95% of the significant ALE values, we determined that the rostral boundary of MPMC was $y = 12$ at $z = 70$, and $y = 26$ at $z = 40$ (Fig. 2, Table 2A). Thus, at certain coordinates in the z dimension, our findings confirm previous suggestions for the rostral boundary of MPMC. However, we found that the rostral boundary of MPMC varied in the z dimension, generally being more caudal in the dorsal segment and rostral in the ventral segment. Although it was not noted in the text, the summary in Fig. 5D of Picard and Strick (1996) also suggests that the rostral boundary of pre-SMA varies in the z dimension similar to the results in the current study.

Caudal limit of MPMC

Caudally, MPMC is bound by SMC in the rostral portion of the paracentral lobule and it has been suggested that this boundary corresponds with the VCP line ($y \cong 23$mm) (Deiber et al., 1999; Chainay et al., 2004). However, it has also been posited that the boundary between MPMC and SMC is unknown due to a lack of macroanatomical and cytoarchitectonic boundaries (Roland and Zilles, 1996; Geyer et al., 2000a), and because the cytoarchitectonic border between areas 4 and 6 is the most variable in the paracentral lobule (Brodmann, 1909; White et al., 1997). Our analysis suggests that the boundary between MPMC and SMC varies in the z dimension, and that this boundary is generally more caudal dorsally than it is ventrally (Fig. 2). Where MPMC was bounded by SMC, our results were within 5mm of the VCP line: where $y = -23$ at $z = 70$, and $y = -28$ at $z = 55$ (Fig. 2). Below $z = 52$, SMC receded laterally and no longer bordered MPMC. The caudal limits of MPMC ventral to this point were $y = -30$ at $z = 50$, and $y = -12$ at $z = 40$. Our results also show that the border between SMA proper and M1 quickly disappears ventral to $z = 55$, where SMC recedes laterally. This boundary may be affected by the disparity in somatotopic data (see Methods, Boundary Estimation) because the somatotopy of the leg occurs in the mesial portion of SMC (Alkadhi et al., 2002a,b) and the caudal portion of MPMC (Mitz and Wise, 1987; Mayer et al., 2001; Fontaine et al., 2002; Chainay et al., 2004). If the lower limb portion of SMC encompasses the full dorso-ventral extent of the paracentral lobule, SMC may extend further rostral and ventral than estimated by our ALE analysis if we were to consider that the ventral limit of the paracentral lobule is $z \cong 47$ (Talairach and Tournoux, 1988). This would cause the boundary line between the two regions to be, in actuality, more vertical than the current findings suggest. However, functional somatotopy studies looking at foot movements indicate that this is not the case

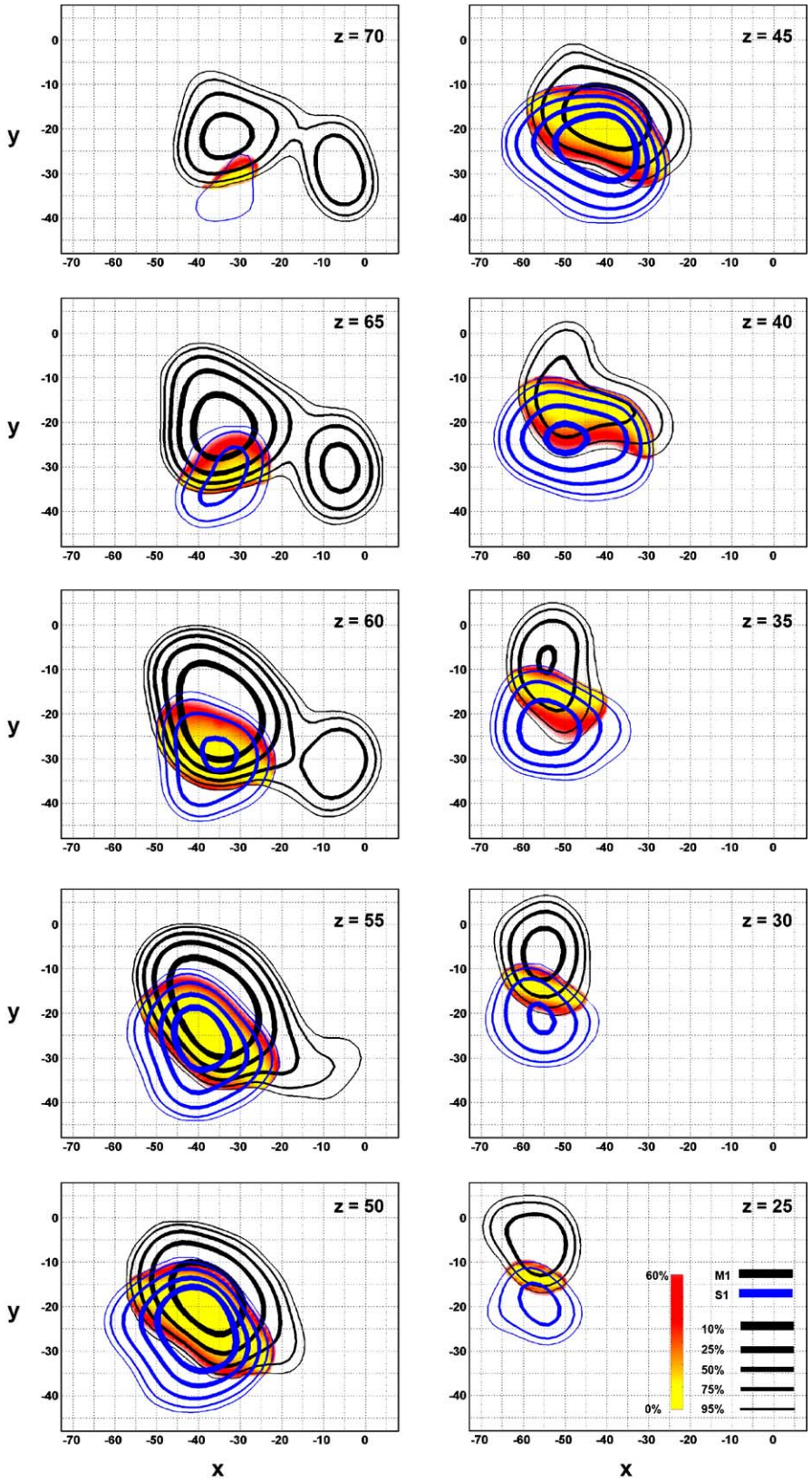

Fig. 5. Contour lines and spatial probability maps between the regions designated as M1 (black) and S1 (blue). Contour lines and difference maps are identical to that described in Fig. 2. Axial slices are shown.

and that activation related to the foot is contained within the dorsal portions of the paracentral lobule—well within our ALE boundaries (Alkadhi et al., 2002a,b). Nevertheless, our data suggest that the border between MPMC and SMC is graded, progressing caudal and ventral through the brain.

Ventral limit of MPMC

It is generally accepted that the border between MPMC and CMA is at the cingulate sulcus with the ventral limit of MPMC being above, and the dorsal limit being buried within the cingulate sulcus (Dum and Strick, 1991; Luppino et al., 1991; Picard and Strick, 1996; Russo et al., 2002). However, the anatomy of the cingulate sulcus is highly variable between subjects (Vogt et al., 1995; Paus et al., 1996), and cellularly the borders between MPMC and CMA can be difficult to define (Russo et al., 2002; Johansen-Berg et al., 2004). The ventral limit of MPMC, as determined by our analysis, varied depending on its rostro-caudal location (Fig. 2). For instance, the ventral limit of pre-SMA was at $z = 33$, the ventral limit where SMA intersects the VCA line was at $z = 40$, and the ventral limit of SMA proper was at $z = 44$. Therefore, our data suggest that the ventral limit is more ventral rostrally than it is caudally, and this finding is consistent with previous depictions (in figures) (Crosson et al., 1999; Deiber et al., 1999; Johansen-Berg et al., 2004). It is interesting to note that these values were ventral to the location of the cingulate sulcus in the Talairach and Tournoux atlas (1988). Based on the above findings, we speculate that a probabilistic comparison of MPMC and CMA would reveal a considerable overlapping area between the two regions.

Lateral limits of SMA

It has been previously noted that there is no mention in classic cytoarchitectonic literature of the differences between the mesial and lateral premotor cortices (Matelli et al., 1991), despite the fact that these regions had been identified as two different cytoarchitectonic areas (Penfield and Welch, 1951; Woolsey et al., 1952). In our literature review, we also found little discussion regarding the location of the border between MPMC and LPMC in humans. In monkeys, the boundary is generally drawn at the spur of the arcuate sulcus and its imaginary caudal extension (Matelli et al., 1985), but resolving this distinction in the human brain is less clear. Our analysis using the ALE method resolves these boundaries at $x = \pm 15$mm (Fig. 3).

Lateral premotor cortex (LPMC)

There are 5 boundaries of importance within LPMC: the boundary between PMd and PMv, the rostral limit of LPMC (the boundaries between FEF dorsally and Broca's area ventrally), the caudal limit of LPMC (the boundary between LPMC and SMC), the medial limit between LPMC and MPMC, and the ventral limit of LPMC. The discussion regarding the mesial boundary of LPMC has already been discussed within the MPMC section, and the discussion regarding the ventral limit of LPMC will be discussed in the SMC section.

PMd vs. PMv

The dorsal and ventral aspects of LPMC have been identified in monkeys as being two separate regions based on cytoarchitectonic and connectional differences subdivided at the spur of the arcuate sulcus and its imaginary caudal extension (Matelli et al., 1985; Barbas and Pandya, 1987). The human anatomical equivalent of this boundary is the virtual continuation of the inferior frontal sulcus, a division that is used by researchers to demarcate the ventral limit of the frontal eye fields (FEF, area 8) (Picard and Strick, 2001) and to differentiate between PMd and PMv (Schubotz and von Cramon, 2003). However, because there are no distinct cellular subdivisions that directly correspond to any macroanatomical landmarks in humans, the precise boundary between the dorsal and ventral sections of LPMC remains uncertain (Geyer et al., 2000a; Picard and Strick, 2001; Schubotz and von Cramon, 2003). The results from our analysis suggest that the boundary between these two regions is between $z = 35$ (medially) and $z = 45$ (laterally) (Fig. 4 at $y = 5$ to -5). These values are in agreement with the location of the virtual continuation of the inferior frontal sulcus as described in the Talairach and Tournoux atlas (1988). However, a comprehensive review of PMv proposed that the boundary between PMd and PMv is at $z = 50$, at the upper limit of FEF (Rizzolatti and Luppino, 2001). While the boundary suggested by Rizzolatti and colleagues (2001) is only 5mm dorsal to our suggested lateral border, it is 15mm dorsal to our suggested medial border. Conceivably, neuroimaging literature has tended to attribute activation to PMd when in all actuality it may have been located in the dorsal rim of the PMv (Schubotz and von Cramon, 2003). Nonetheless, our data suggest that the PMd/PMv border is more ventral medially than it is laterally.

Rostral limits of LPMC

It is has been suggested that the rostral limit of LPMC is the precentral sulcus (Picard and Strick, 1996; Roland and Zilles, 1996; Moore et al., 2000; Simon et al., 2002). LPMC is bounded by FEF (area 8) where the precentral sulcus intersects the superior frontal sulcus and recent work suggests that FEF is contained in the depths of the precentral sulcus (Rosano et al., 2002). On the other hand, two previous reviews of functional imaging data showed that FEF appeared to include the rostral most portion of the precentral gyrus (Paus, 1996; Petit et al., 1999). The findings from these two reviews indicated that the boundary between areas 8 and 6 might be positioned caudal to the precentral sulcus, on the rostral portion of the precentral gyrus. In comparison with our results, we found that 30 out of the 40 FEF coordinates listed in these two reviews fell within the 95th percentile of LPMC. Since it has been suggested that the tasks used in the studies investigating FEF could activate both visual and visuomotor neurons (Blanke et al., 2000), it is possible that there is an area of functional overlap between the eye fields and manual premotor area, or possibly an individuated visuomotor field. Supporting this hypothesis, recent fMRI studies using a precision grip task have demonstrated that the visuomotor process occurs in the rostral portions of the precentral gyrus (Vaillancourt et al., 2003; Vaillancourt et al., 2006). Therefore, the current findings suggest that the LPMC region determined by our ALE method appears to include activations that some may consider to be FEF.

Ventrally, the rostral aspect of LPMC is bounded by area 44. Area 44 is the opercular portion of the inferior frontal gyrus and is traditionally referred to as the caudal portion of Broca's area (Brodmann, 1909). The cytoarchitectonic borders between areas 44 and 6 do not reliably coincide with identifiable macroscopic features, and it has been suggested that this border cannot be determined solely on the basis of macroanatomical landmarks (Amunts et al., 1999). Additionally, recent work investigating the

motor functions of Broca's area has suggested that this region may be the human equivalent of monkey area F5 (Rizzolatti et al., 1998; Amunts et al., 1999) and that it could be considered part of PMv (Rizzolatti et al., 2002; Schubotz and von Cramon, 2003; Binkofski and Buccino, 2004). For these reasons, the rostral limit of PMv is not well established. Our results show that the rostral limit of LPMC varies between $y = 10$ and 20 (Table 4A). These findings appear to be located on the opercular portion of the inferior frontal gyrus as determined by the Talairach and Tournoux atlas (1988). For example, the Talairach and Tournoux atlas shows that the rostro-caudal extent of the ventral precentral sulcus ranged between $y = -2$ and $y = 10$, and was situated caudally with respect to the rostral limit of our LPMC region. To compare this boundary to previously reported data for Broca's area, we inspected 62 coordinates from 18 of the articles from this meta-analysis (Appendix A with a single asterisk) that reported Broca's area during hand or arm movement tasks. The coordinates from these 18 articles ranged from $y = -3$ to $y = 38$, with a mean of $y = 10$ in the rostro-caudal plane, and 47 out of the 62 coordinates fell within the 95th percentile of our LMPC region. We also examined 19 coordinates reported for Broca's area from 9 additional articles that had investigated speech/oral motor tasks (Schumacher et al., 1996; Tzourio et al., 1998; Kang et al., 1999; Hernandez et al., 2001; Palmer et al., 2001; Gruber and von Cramon, 2003; Li et al., 2003; Siok et al., 2003; Tan et al., 2003). The area 44 coordinates from these 9 articles ranged from $y = 4$ to $y = 18$, with a peak of $y = 11$ in the rostro-caudal dimension, and 17 out of the 19 coordinates fell within the 95th percentile of our LMPC region. It is important to note that out of the 14 studies involving speech/oral–motor tasks included in our meta-analysis, none identified activation in PMv or LPMC. Therefore, the rostral extent of our ventral LPMC area was not influenced by functional activity related to speech. Based on these observations, it appears that researchers may consider the opercular portion of the inferior frontal gyrus to be part of PMv.

Caudal limit of LPMC

It is widely accepted that there is a gradual cytoarchitectonic border between areas 6 and 4 (Roland and Zilles, 1996) and the criteria for this border is the change in the number and density of Betz cells in layer V (White et al., 1997; Wang et al., 2002). Generally, M1 is said to reside within the depths of the central sulcus (Geyer et al., 2000a). However, there are reports that M1 covers the entirety of the precentral gyrus (Brodmann, 1909; White et al., 1997), or simply portions of the exposed surface of the precentral gyrus (Rademacher et al., 2001b) in the dorsal-most aspect of the cortex. These ambiguities have forced imaging researchers to delineate an arbitrary boundary between LPMC and SMC, such as the definition that this boundary is at the caudal 2/3rds of the precentral gyrus (Alkadhi et al., 2002a; Alkadhi et al., 2002b), or at the rostral lip of the central sulcus (Fink et al., 1997). From this meta-analysis, we were able to locate the line of equal probability between these two regions—a guide that will be useful for predicting this border in stereotaxic space. In the axial plane ($z = 55$), this boundary is more rostral laterally ($x = -50$, $y = -5$) than it is medially ($x = -20$, $y = -15$) (Fig. 2). We also found that the individual centers of LPMC and SMC are close in proximity, resulting in a large overlapping area between the two regions. It is possible that this overlap is due to the variability inherent in the shape and extent of the central sulcus within (White et al., 1997; Rademacher et al., 2001b; Fesl et al., 2003) and between subjects (White et al., 1997; Yousry et al., 1997; Roland and Zilles, 1998; Moore et al., 2000; Rademacher et al., 2001b).

Sensorimotor cortex (SMC)

There are 4 boundaries of importance within SMC: the boundary between M1 and S1, the rostral limit of SMC, the caudal limit of S1, and the ventral limit of SMC. The rostral limit of SMC was discussed within the MPMC and LPMC sections.

M1 vs. S1

The cytoarchitectonic border between M1 and S1 (area 3) is well defined and located in the depths of the central sulcus (Geyer et al., 1997, 2000a; Moore et al., 2000; Rademacher et al., 2001b). However, despite the fact that the division between M1 and S1 is cytoarchitectonically considered one of the most consistent boundaries in the human brain (Roland and Zilles, 1996; Geyer et al., 1997; Rademacher et al., 2001b), we found that the overlap between these regions was the largest overlap of all the boundaries in this study (Table 3). This overlap is likely due to the large interindividual variability of the central sulcus (Geyer et al., 1997, 2000b; White et al., 1997; Moore et al., 2000; Rademacher et al., 2001b) combined with the difficulty of normalizing a highly variable landmark such as the central sulcus (Woods, 1996). Furthermore, these factors combined with the fact that M1 and S1 are generally co-activated, make it difficult to differentiate between these two regions in stereotaxic space. These complications are evidenced by the finding that the isocenters of M1 and S1 completely overlap (Fig. 5, $z = 55$). Nevertheless, using boundaries based on the overlap between SMC and LPMC and M1 and S1, the volume derived for M1 is 33.4cm^3. Rademacher et al. (2001b) estimated the grey matter of Brodmann area 4 to be approximately 10.9cm^3, and Zhou et al. (2005) estimated the grey and white matter of the precentral gyrus to be 33.5cm^3. Considering that our method cannot distinguish between grey and white matter, our estimate for the volume of M1 appears to be in line with these reports. Ultimately, our analysis describes the variability between M1 and S1 in stereotaxic space, and will serve as a functional guide complementing the previously described cytoarchitectonical and macroanatomical variability of this region.

Caudal limit of S1

The caudal edge of area 2 is bound by three different cytoarchitectonic regions: the pre-parietal area 5 dorsally, the superior parietal area centrally, and the supramarginal area 40 ventrally (Brodmann, 1909). The caudal edge of area 2 is generally considered to be in the postcentral sulcus (Brodmann, 1909; Geyer et al., 2000b; Moore et al., 2000; Grefkes et al., 2001), although this border is topographically variable between the fundus of the postcentral sulcus and several millimeters above it on the caudal wall (Brodmann, 1909; Geyer et al., 2000b; Moore et al., 2000; Grefkes et al., 2001). Because the literature regarding this boundary is sparse, our analysis will be a useful measure for determining the caudal boundary of S1 in Talairach space.

Ventral limits of LPMC and SMC

The ventral limit of M1 has been reported as being situated just above the Sylvian Fissure (Woolsey et al., 1979; Corfield et al., 1999), or varying as much as 4cm dorsally (Brodmann, 1909; Urasaki et al., 1994; Geyer et al., 2000b). Similarly, the ventral limit of S1 has been shown to correspond to the same dorso-ventral

position as M1, immediately caudal to M1 at the base of the postcentral gyrus (Boling et al., 2002). It also has been noted that the ventral limit of area 2 may or may not coincide with the Sylvian Fissure, a finding that was independent of whether or not the postcentral sulcus reached the Sylvian Fissure (Grefkes et al., 2001). Our current findings showed that the ventral limit of SMC was approximately $z = 20$ (Table 5A), just below peak z activations that have been reported (between $z = 24$ and 40) for the most ventral part of area 4 (i.e.. the motor tongue area) (Fox et al., 2001; Alkadhi et al., 2002a; Turkeltaub et al., 2002; Ehrsson et al., 2003b; Fesl et al., 2003). This location is just above the Sylvian Fissure based on the Talairach and Tournoux atlas (1988). We found little information in the literature regarding the ventral boundary of LPMC. The ventral extent of LPMC based on our ALE method was at $z = -2$ (Fig. 4, $y = 5$). This location corresponds to the ventral limits of the precentral gyrus based on the Talairach and Tournoux atlas (1988). Because the Sylvian Fissure is an inconsistent macroanatomical boundary on the order of several centimeters, our findings are important as they suggest guidelines regarding the lower limits of SMC and LPMC in stereotaxic space.

Computational issues related to the ALE method

It should be noted that there are several computational issues that are inherent to the ALE method which affect the spatial distribution of an ROI. First, the spatial distribution is affected by the sigma value chosen to represent the standard deviation associated with each data point. A large sigma value will result in a larger and smoother region. Second, the number of coordinates needed to obtain an accurate representation of a region depends on its shape and volume. This manuscript looks at 6 regions, all with differing volumes. A larger number of coordinates would be required to accurately estimate a region with a large volume such as LPMC, compared to a region with a small volume, such as SMA proper. Because the precise volumes of these regions are unknown a priori, we are unable to determine the number of data points that would be required per region in order to generate an accurate representation of its spatial extent. Third, this method is inherently sensitive to the number of data points sampled within a given volume. When the number of data points sampled from within a particular ROI is increased, more voxels become significant and the overall volume increases. This phenomenon occurs because the ALE values of the voxels in and around the ROI grow at a faster rate than do the ALE values determined by the null hypothesis. Lastly, the number of significant ALE values is dependent upon the threshold chosen. As such, it is essential to carefully check the results of the probabilistic analysis against known anatomical landmarks as done in this manuscript.

Summary and conclusions

This meta-analysis compiled three-dimensional coordinates in stereotaxic space from six principle cortical motor ROIs across 126 articles from the PET and fMRI literature. The ALE method was used to quantify probability maps that describe the outer limits and boundaries for SMA, pre-SMA, PMd, PMv, M1, and S1. In some cases, such as the boundary between SMA and pre-SMA, our findings have confirmed previous suggestions in the literature. In others, our findings provide estimates in Talairach space that will complement suggested anatomical boundaries, such as the boundary between M1 and S1, the posterior limit of S1, the ventral limits of MPMC, SMC, and LPMC. Lastly, our findings provide novel estimates in Talairach space for boundaries that do not have anatomical equivalents such as the rostral, caudal, and lateral limits of MPMC, the anterior limits of LPMC, the boundary between PMd and PMv, and the boundary between LPMC and SMC. Additionally, our findings demonstrate that there does not appear to be a distinct one-dimensional boundary at any one x, y, or z coordinate. Rather, there is a gradient that varies in three dimensions separating each ROI. For instance, the border between PMd and PMv is not a horizontal line, but instead is best represented by a boundary line that traverses from a position that is ventral at its lateral limit and dorsal at its medial limit.

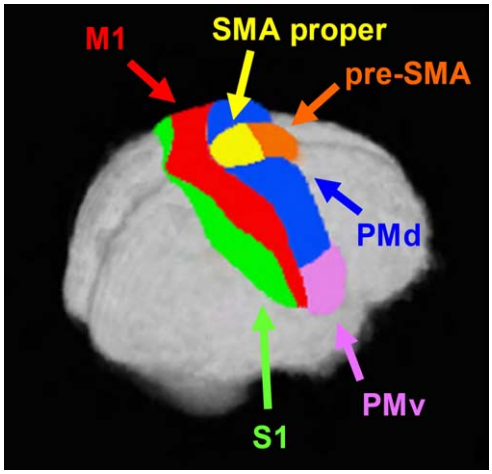

Fig. 6. Human Motor Area Template drawn in AFNI based upon data generated from our probability distributions along with previously established anatomical criteria. The regions shown are pre-SMA (orange), SMA proper (yellow), PMd (blue), PMv (magenta), M1 (red) and S1 (green).

While the limitations of Talairach space have been previously noted (Woods, 1996; Brett et al., 2002), there are also several benefits to using a standardized stereotaxic space. In particular, normalization provides a common framework that can be used to compare results from different laboratories. We have used the outcomes from our ALE analysis in combination with previously suggested anatomical guidelines to draw the Human Motor Area Template (HMAT) for these six motor and premotor areas in Talairach space (Fig. 6). HMAT can be obtained through e-mail from the corresponding author. This template is not meant to serve as a gold standard for imaging studies of the motor system, but rather as a starting point such that data from future neuroimaging studies can be more accurately quantified and described in Talairach coordinate space. For example, we recognize that additional work on the cingulate area would make an important contribution. In conclusion, we believe this meta-analysis will add cohesiveness to the neuroimaging literature by facilitating a better understanding of motor systems neuroscience, while also advancing our understanding of the effects of physical rehabilitation, pharmacological interventions, and surgical treatment on impaired brain function.

Acknowledgments

This research was supported in part by grants from the National Institutes of Health (R01-NS-52318, R01-NS-28127, R01-NS-40902). We thank Drs. John Sweeney and Colum MacKinnon for their thoughts and invaluable comments on this manuscript.

Appendix A. Summary of studies

First author	*N*	Scanner	Body part	pre-SMA	SMA proper	MPMC	PMd	PMv	LPMC	M1	S1	SMC
Adam (2003)*	14	fMRI (1.5T)	hand (key press)			√	√		√			√
Alkadhi (2002a)	12	fMRI (1.5T)	hand/wrist (flexion/extension), elbow (flexion/extension), hand (open/close), finger (tapping), ankle (plantar/dorsal flexion), tongue (bilateral horizontal movements)							√		
Alkadhi (2002b)	12	fMRI (1.5T)	hand/wrist (flexion/extension), elbow (flexion/extension), hand (open/close), finger (tapping), ankle (plantar/dorsal flexion), tongue (bilateral horizontal movements)							√		
Baraldi (1999)	10	fMRI (1.5T)	hand (sequential finger tapping)			√			√	√	√	
Binkofski (1999)	5	fMRI (1.5T)	hand (object manipulation)				√	√				
Binkofski (2000)*	6	fMRI (1.5T)	finger (trajectories)			√	√	√				√
Bischoff-Grethe (2002)	10	fMRI (1.5T)	finger (button press)			√			√	√		
Boecker (1998)	7	PET	hand (sequential finger tapping)	√	√	√			√	√	√	
Calhoun (2002)	12	fMRI (1.5T)	hand (driving, game controller)						√			
Carel (2000)	12	fMRI (1.5T)	hand (flexion/extension)			√						√
Choi (2001)	10	fMRI (1.5T)	hand (gesturing)			√			√	√		
Christensen (2000)	7	PET	legs (bicycling)			√				√	√	
Corfield (1999)	8	fMRI (2T)	tongue (contraction)			√						√
Culham (2003)	7	fMRI (4T)	arm (reaching), hand (grasping)							√		
Cunnington (2002)	12	fMRI (3T)	hand (sequential button press)			√				√		
Dassonville (2001)	8	fMRI (4T)	hand (joystick)	√			√	√				
de Jong (1999)**	15,15	PET	hand (drawing)		√	√			√			
de Jong (2001)	7	PET	arm (reaching)					√				
de Weerd (2003)	5	fMRI (1.5T)	finger/hand (tapping/opposition)	√	√				√	√		
Debaere (2001)	6	fMRI (1.5T)	hand/foot (flexion/extension)		√				√			√
Debaere (2003)	12	fMRI (1.5T)	hand (movements-internal vs. external generation)			√		√				
Deiber (1998)*	10	PET	finger/hand (moving/tapping)	√					√			
Desmurget (2001)	7	PET	arm (reaching)							√		√
Deuchert (2002)	6	fMRI (1.5T)	finger (electrical stimulus)								√	
Dhamala (2003)	18	fMRI (1.5T)	finger (rhythmic tapping)							√		
Dreher and Grafman (2002)*	8	fMRI (1.5T)	hand (button press)	√			√			√		
Ehrsson (2000)	5	fMRI (1.5T)	hand (grip)			√	√	√		√	√	√
Ehrsson (2001)*	6	fMRI (1.5T)	hand (grip)			√		√		√		√
Ehrsson (2003a)	6	fMRI (1.5T)	finger/hand (grasping)			√		√				√
Ehrsson (2003b)	6	fMRI (1.5T)	finger/toe (flexion/extension), tongue (horizontal movement)			√	√			√		
Ellermann (1998)*	9	fMRI (4T)	hand (joystick)			√			√	√	√	
Ferrandez (2003)	11	fMRI (1.5T)	finger (keypress)			√			√			
Fesl (2003)	11	fMRI (1.5T)	tongue (horizontal movement)			√						√
Foltys (2003)	8	fMRI (1.5T)	hand (grip)			√				√	√	
Frutiger (2000)	25	PET	hand (drawing)			√				√		
Ghilardi (2000)	12	PET	arm (reaching)			√			√	√	√	
Grafton (2002)	8	PET	finger/hand (button press)			√				√		
Grezes (2003a)	12	fMRI (2T)	finger/hand (grip)				√					
Grezes (2003b)	12	fMRI (2T)	hand (grip)				√	√				
Hamzei (2002a)**	6,6	fMRI (1.5T)	hand (writing)		√				√	√	√	
Hamzei (2002b)	6	fMRI (1.5T)	hand (grip)				√					√

(continued on next page)

Appendix A (*continued*)

First author	*N*	Scanner	Body part	pre-SMA	SMA proper	MPMC	PMd	PMv	LPMC	M1	S1	SMC
Haslinger (2002)	8	fMRI (1.5T)	hand (sequential finger tapping)			√	√	√			√	√
Horwitz (2000)	13	PET	finger/hand (abduction/elevation)						√		√	
Indovina and Sanes (2001a)*	9	fMRI (1.5T)	finger/hand (button press)	√	√		√	√	√	√	√	
Indovina and Sanes (2001b)	10	fMRI (1.5T)	finger/hand (flexion/extension)			√				√		
Ino (2003)*	18	fMRI (1.5T)	hand (drawing)	√			√			√		
Inoue (1998)	9	PET	hand/arm (reaching/pointing)			√				√	√	
Inoue (2000)	6	PET	arm (reaching)		√		√					
Jancke (2000a)	6	fMRI (1.5T)	hand (sequential button press)	√				√				
Jancke (2000b)	8	fMRI (1.5T)	finger (tapping)			√	√	√		√	√	
Jantzen (2002)	8	fMRI (1.5T)	hand (grip)			√				√		
Jenkins (1997)	6	PET	hand (joystick)			√			√			√
Jenkins (2000)*	6	PET	finger (tapping)	√		√			√			√
Johannsen (2001)	8	PET	foot/ankle (voluntary contractions)			√			√	√	√	
Johansen-Berg and Matthews (2002)	12	fMRI (3T)	tongue (counting)/finger (button press)	√	√		√		√	√	√	√
Johnson (2002)*	8	fMRI (1.5T)	hand (grip selection)			√	√		√	√	√	
Joliot (1999)	8	PET	hand (sequential finger tapping)			√			√	√	√	
Kawashima (2000a)	8	fMRI (1.5T)	tongue (articulation)/finger (tapping)			√			√			√
Kawashima (2000b)	9	PET	hand (writing)			√	√	√		√		
Kinoshita (2000)	10	PET	hand (grip)			√				√	√	√
Kobayashi (2003)	10	fMRI (1.5T)	finger (tapping)							√		
Koechlin (2000)*	6	fMRI (1.5T)	hand (button press)	√	√				√			
Koski (2002)*	14	fMRI (3T)	finger (movements)				√					√
Krams (1998)*	8	PET	hand (key press)						√	√	√	
Kuhtz-Buschbeck (2001)	8	fMRI (1.5T)	finger/hand (grip)			√		√		√		√
Lacquaniti (1997)*	8	PET	arm (reaching)			√			√			√
Lafleur (2002)	9	PET	foot (sequences, flexion/extension)	√	√		√			√		
Lamm (2001)	13	fMRI (3T)	finger (button press)			√			√			
Leube (2003)	18	fMRI (1.5T)	hand (open/close)			√			√		√	
Liddle (2001)	16	fMRI (1.5T)	finger (finger tap)			√		√	√	√	√	
Lotze (2000)	7	fMRI (1.5T)	tongue (articulation)							√	√	√
Lotze (2003)	25	fMRI (1.5T)	wrist (flexion/extension)							√	√	
Maguire (2003)	6	fMRI (1.5T)	finger (button press)			√						
Malouin (2003)	6	PET	legs (locomotion imagery)	√	√		√				√	
Manthey (2003)	12	fMRI (3T)	fingers (button press)	√				√				
Martin (2001)	14	fMRI (4T)	tongue/throat (swallowing)								√	√
Matsuo (2003)	12	fMRI (3T)	finger (sensory discrimination)	√	√				√	√	√	
Mattay (1998)	8,7	fMRI (1.5T)	hand/finger (sequential tapping)			√			√	√	√	
Mayville (2002)	9	fMRI (1.5T)	hand (squeezing)			√			√			√
Muley (2001)**	10,10, 20	PET	hand (grip)			√						√
Muller (2002)*	7	fMRI (1.5T)	hand (sequential finger tapping)			√		√	√	√	√	
Nakai (2003)	10	fMRI (3T)	finger (tapping)			√			√			√
Nowak (1999)	8	PET	hand (grip)			√						√
Nyberg (2001)	10	PET	hand, arm, shoulder (random tasks)						√			√
Oishi (2003)	12	fMRI (3T)	foot/ankle (plantar response)			√				√	√	

Appendix A (*continued*)

Penhune and Doyon (2002)	9	PET	finger/hand (tapping)			√			√	√		
Rao (1997)*	13	fMRI (1.5T)	finger (key press/tapping)			√				√		
Rauch (1997)	10	fMRI (1.5T)	hand (key press)						√			
Riecker (2002)	12	FMRI (1.5T)	tongue (syllable production)			√				√		
Riecker (2003)	8	fMRI (1.5T)	finger (tapping/button)	√	√							√
Rotte (2002)	9	fMRI (1.5T)	finger, toe, tongue, eye, knee, diaphragm/pelvis (muscle contractions, simple motor tasks)			√				√		
Rowe (2002)	12	fMRI (2T)	hand (sequential finger tapping)			√			√	√		
Sadato (1997)**	12,9	PET	hand (sequential finger tapping)			√	√	√				√
Saito (2003)	11	fMRI (3T)	finger/hand (tactile matching)			√	√					√
Sakai (1999)	6	fMRI (1.5T)	finger (button press)						√			
Sakai (2000)	6	fMRI (1.5T)	hand/finger (button press)	√	√				√	√		
Schubotz and Von Cramon (2001)	12	fMRI (3T)	hand (sequential finger tapping)	√	√		√	√		√	√	
Schubotz and Von Cramon (2002a)	18	fMRI (3T)	finger/hand (button press)	√	√	√	√	√				
Schubotz and Von Cramon (2002b)**	12,5	fMRI (3T)	finger (button press)	√			√	√	√			
Siebner (2001)	10	PET	hand (handwriting)		√	√	√	√	√			√
Solodkin (2001)	13	fMRI (1.5T)	hand (sequential finger tapping)			√			√	√	√	
Staines (2002)**	6,12	fMRI (1.5T)	finger (tapping/electrode stimulus), tongue (counting)			√			√			
Stephan (2002)	9	PET	finger tapping (sequencing)						√			
Stippich (2002)	14	fMRI (1.5T)	tongue (up down), finger (tapping), toe (flexion/ extension)									√
Stoeckel (2003)	7	fMRI (1.5T)	finger/hand (sensory discrimination)				√	√		√	√	
Sugio (2003)	13	fMRI (1.5T)	finger/hand (grasping)			√				√	√	
Toma (2003)	13	fMRI (3T)	finger (button press)			√			√			√
Toni (1998)	3	fMRI (2T)	hand (keypad sequences)			√			√	√	√	
Toni and Passingham (1999)	10	PET	hand (sequential button press)						√	√	√	
Toni (2001a)	7	fMRI (2T)	finger/hand (button press)					√				
Toni (2001b)	12	PET	hand (gestures)			√		√				
Toni (2002)	6	fMRI (1.5T)	finger/hand (button press)			√	√		√	√	√	
Tracy (2001)	9	fMRI (1.5T)	arm (supination/pronation)			√			√	√		
Tracy (2003)	15	fMRI (1.5T)	hand (knot tying)						√	√		
Turner (1998)	9	PET	arm/shoulder (joystick tracking)			√	√		√			√
Ullen (2003)	14	fMRI (1.5T)	finger (tapping)	√	√	√	√	√	√	√		
Ullsperger and Von Cramon (2001)*	12	fMRI (3T)	hand (button press)	√	√				√	√		
Vaillancourt (2003)	10	fMRI (3T)	finger (pinch grip)			√			√	√	√	
van Mier (1998)*	32	PET	hand (drawing)			√			√	√	√	
Viviani (1998)	10	PET	hand (rotation)			√			√	√		
Watanabe (2002)	11	fMRI (1.5T)	finger/hand (button press)				√	√				√
Weiss (2003)	12	PET	arm (reaching/pointing)						√			√
Wildgruber (2001)	10	fMRI (1.5T)	tongue (syllables)			√				√		
Winstein (1997)	6	PET	hand (stylus tapping)	√	√	√	√	√		√		
Winterer (2002)	6	fMRI (3T)	thumb (button press)			√				√		
Yoo (2003)	13	fMRI (3T)	hand (tactile stimulation)			√			√		√	

N=Number of participants, T=Telsa. * Indicates studies that included BA 44 coordinates. ** Indicates an article that contained more than one set of experiments with different numbers of subjects.

References

Adam, J.J., Backes, W., Rijcken, J., Hofman, P., Kuipers, H., Jolles, J., 2003. Rapid visuomotor preparation in the human brain: a functional MRI study. Cogn. Brain Res. 16, 1–10.

Alkadhi, H., Crelier, G.R., Boendermaker, S.H., Golay, X., Hepp-Reymond, M.C., Kollias, S.S., 2002a. Reproducibility of primary motor cortex somatotopy under controlled conditions. Am. J. Neuroradiol. 23, 1524–1532.

Alkadhi, H., Crelier, G.R., Boendermaker, S.H., Hepp-Reymond, M.C., Kollias, S.S., 2002b. Somatotopy in the ipsilateral primary motor cortex. NeuroReport 13, 2065–2070.

Amunts, K., Schleicher, A., Burgel, U., Mohlberg, H., Uylings, H.B., Zilles, K., 1999. Broca's region revisited: cytoarchitecture and intersubject variability. J. Comp. Neurol. 412, 319–341.

Amunts, K., Malikovic, A., Mohlberg, H., Schormann, T., Zilles, K., 2000. Brodmann's areas 17 and 18 brought into stereotaxic space — where and how variable? NeuroImage 11, 66–84.

Baraldi, P., Porro, C.A., Serafini, M., Pagnoni, G., Murari, C., Corazza, R., Nichelli, P., 1999. Bilateral representation of sequential finger movements in human cortical areas. Neurosci. Lett., 269.

Barbas, H., Pandya, D.N., 1987. Architecture and frontal cortical connections of the premotor cortex (area 6) in the rhesus monkey. J. Comp. Neurol. 256, 211–228.

Binkofski, F., Buccino, G., 2004. Motor functions of the Broca's region. Brain Lang. 89, 362–369.

Binkofski, F., Buccino, G., Stephan, K.M., Rizzolatti, G., Seitz, R.J., Freund, H.J., 1999. A parieto-premotor network for object manipulation: evidence from neuroimaging. Exp. Brain Res. 128, 210–213.

Binkofski, F., Amunts, K., Stephan, K.M., Posse, S., Schormann, T., Freund, H.J., Zilles, K., Seitz, R.J., 2000. Broca's region subserves imagery of motion: a combined cytoarchitectonic and fMRI study. Hum. Brain Mapp. 11, 273–285.

Bischoff-Grethe, A., Ivry, R.B., Grafton, S.T., 2002. Cerebellar involvement in response reassignment rather than attention. J. Neurosci. 22, 546–553.

Blanke, O., Spinelli, L., Thut, G., Michel, C.M., Perrig, S., Landis, T., Seeck, M., 2000. Location of the human frontal eye field as defined by electrical cortical stimulation: anatomical, functional and electrophysiological characteristics. NeuroReport 11, 1907–1913.

Boecker, H., Dagher, A., Ceballos-Baumann, A.O., Passingham, R.E., Samuel, M., Friston, K.J., Poline, J., Dettmers, C., Conrad, B., Brooks, D.J., 1998. Role of the human rostral supplementary motor area and the basal ganglia in motor sequence control: investigations with H2 15O PET. J. Neurophysiol. 79, 1070–1080.

Boling, W., Reutens, D.C., Olivier, A., 2002. Functional topography of the low postcentral area. J. Neurosurg. 97, 388–395.

Brett, M., Johnsrude, I.S., Owen, A.M., 2002. The problem of functional localization in the human brain. Nat. Rev., Neurosci. 3, 243–249.

Brodmann, K., 1909. Brodmann's Localisation in the Cerebral Cortex. Imperial College Press, London.

Calhoun, V.D., Pekar, J.J., McGinty, V.B., Adali, T., Watson, T.D., Pearlson, G.D., 2002. Different activation dynamics in multiple neural systems during simulated driving. Hum. Brain Mapp. 17, 141–142.

Carel, C., Loubinoux, I., Boulanouar, K., Manelfe, C., Rascol, O., Celsis, P., Chollet, F., 2000. Neural substrate for the effects of passive training on sensorimotor cortical representation: a study with functional magnetic resonance imaging in healthy subjects. J. Cereb. Blood Flow Metab. 20, 478–484.

Chainay, H., Krainik, A., Tanguy, M.L., Gerardin, E., Le Bihan, D., Lehericy, S., 2004. Foot, face and hand representation in the human supplementary motor area. NeuroReport 15, 765–769.

Chiavaras, M.M., LeGoualher, G., Evans, A., Petrides, M., 2001. Three-dimensional probabilistic atlas of the human orbitofrontal sulci in standardized stereotaxic space. NeuroImage 13, 479–496.

Choi, S.H., Na, D.L., Kang, E., Lee, K.M., Lee, S.W., Na, D.G., 2001. Functional magnetic resonance imaging during pantomiming tool-use gestures. Exp. Brain Res. 139, 311–317.

Christensen, L.O., Johannsen, P., Sinkjaer, T., Petersen, N., Pyndt, H.S., Nielsen, J.B., 2000. Cerebral activation during bicycle movements in man. Exp. Brain Res. 135, 66–72.

Corfield, D.R., Murphy, K., Josephs, O., Fink, G.R., Frackowiak, R.S., Guz, A., Adams, L., Turner, R., 1999. Cortical and subcortical control of tongue movement in humans: a functional neuroimaging study using fMRI. J. Appl. Physiol. 86, 1468–1477.

Cox, R.W., Jesmanowicz, A., Hyde, J.S., 1995. Real-time functional magnetic resonance imaging. Magn. Reson. Med. 33, 230–236.

Crosson, B., Sadek, J.R., Bobholz, J.A., Gokcay, D., Mohr, C.M., Leonard, C.M., Maron, L., Auerbach, E.J., Browd, S.R., Freeman, A.J., Briggs, R.W., 1999. Activity in the paracingulate and cingulate sulci during word generation: an fMRI study of functional anatomy. Cereb. Cortex 9, 307–316.

Culham, J.C., Danckert, S.L., DeSouza, J.F., Gati, J.S., Menon, R.S., Goodale, M.A., 2003. Visually guided grasping produces fMRI activation in dorsal but not ventral stream brain areas. Exp. Brain Res. 153, 180–189.

Cunnington, R., Windischberger, C., Deecke, L., Moser, E., 2002. The preparation and execution of self-initiated and externally-triggered movement: a study of event-related fMRI. NeuroImage 15, 373–385.

Dassonville, P., Lewis, S.M., Zhu, X.H., Ugurbil, K., Kim, S.G., Ashe, J., 2001. The effect of stimulus-response compatibility on cortical motor activation. NeuroImage 13, 1–14.

de Jong, B.M., Frackowiak, R.S., Willemsen, A.T., Paans, A.M., 1999. The distribution of cerebral activity related to visuomotor coordination indicating perceptual and executional specialization. Cogn. Brain Res. 8, 45–59.

de Jong, B.M., van der Graaf, F.H., Paans, A.M., 2001. Brain activation related to the representations of external space and body scheme in visuomotor control. NeuroImage 14, 1128–1135.

De Weerd, P., Reinke, K., Ryan, L., McIsaac, T., Perschler, P., Schnyer, D., Trouard, T., Gmitro, A., 2003. Cortical mechanisms for acquisition and performance of bimanual motor sequences. NeuroImage 19, 1405–1416.

Debaere, F., Swinnen, S.P., Beatse, E., Sunaert, S., Van Hecke, P., Duysens, J., 2001. Brain areas involved in interlimb coordination: a distributed network. NeuroImage 14, 947–958.

Debaere, F., Wenderoth, N., Sunaert, S., Van Hecke, P., Swinnen, S.P., 2003. Internal vs. external generation of movements: differential neural pathways involved in bimanual coordination performed in the presence or absence of augmented visual feedback. NeuroImage 19, 764–776.

Deiber, M.P., Ibanez, V., Honda, M., Sadato, N., Raman, R., Hallett, M., 1998. Cerebral processes related to visuomotor imagery and generation of simple finger movements studied with positron emission tomography. NeuroImage 7, 73–85.

Deiber, M.P., Honda, M., Ibanez, V., Sadato, N., Hallett, M., 1999. Mesial motor areas in self-initiated versus externally triggered movements examined with fMRI: effect of movement type and rate. J. Neurophysiol. 81, 3065–3077.

Desmurget, M., Grea, H., Grethe, J.S., Prablanc, C., Alexander, G.E., Grafton, S.T., 2001. Functional anatomy of nonvisual feedback loops during reaching: a positron emission tomography study. J. Neurosci. 21, 2919–2928.

Deuchert, M., Ruben, J., Schwiemann, J., Meyer, R., Thees, S., Krause, T., Blankenburg, F., Villringer, K., Kurth, R., Curio, G., Villringer, A., 2002. Event-related fMRI of the somatosensory system using electrical finger stimulation. NeuroReport 13, 365–369.

Dhamala, M., Pagnoni, G., Wiesenfeld, K., Zink, C.F., Martin, M., Berns, G.S., 2003. Neural correlates of the complexity of rhythmic finger tapping. NeuroImage 20, 918–926.

Dreher, J.C., Grafman, J., 2002. The roles of the cerebellum and basal ganglia in timing and error prediction. Eur. J. Neurosci. 16, 1609–1619.

Dum, R.P., Strick, P.L., 1991. The origin of corticospinal projections from the premotor areas in the frontal lobe. J. Neurosci. 11, 667–689.

Duncan, J., Seitz, R.J., Kolodny, J., Bor, D., Herzog, H., Ahmed, A.,

Newell, F.N., Emslie, H., 2000. A neural basis for general intelligence. Science 289, 457–460.
Ehrsson, H.H., Fagergren, A., Jonsson, T., Westling, G., Johansson, R.S., Forssberg, H., 2000. Cortical activity in precision- versus power-grip tasks: an fMRI study. J. Neurophysiol. 83, 528–536.
Ehrsson, H.H., Fagergren, E., Forssberg, H., 2001. Differential fronto-parietal activation depending on force used in a precision grip task: an fMRI study. J. Neurophysiol. 85, 2613–2623.
Ehrsson, H.H., Fagergren, A., Johansson, R.S., Forssberg, H., 2003a. Evidence for the involvement of the posterior parietal cortex in coordination of fingertip forces for grasp stability in manipulation. J. Neurophysiol. 90, 2978–2986.
Ehrsson, H.H., Geyer, S., Naito, E., 2003b. Imagery of voluntary movement of fingers, toes, and tongue activates corresponding body-part-specific motor representations. J. Neurophysiol. 90, 3304–3316.
Ellermann, J.M., Siegal, J.D., Strupp, J.P., Ebner, T.J., Ugurbil, K., 1998. Activation of visuomotor systems during visually guided movements: a functional MRI study. J. Magn. Reson. 131, 272–285.
Evans, A.C., Kamber, M., Collins, D.L., Macdonald, D., 1994. An MRI-based probabilistic atlas of neuroanatomy. In: Shorvon, S., Fish, D., Andermann, F., Bydder, G., Stefan, H. (Eds.), Magnetic Resonance Scanning and Epilepsy, vol. 264. Plenum Press, pp. 263–274.
Ferrandez, A.M., Hugueville, L., Lehericy, S., Poline, J.B., Marsault, C., Pouthas, V., 2003. Basal ganglia and supplementary motor area subtend duration perception: an fMRI study. NeuroImage 19, 1532–1544.
Fesl, G., Moriggl, B., Schmid, U.D., Naidich, T.P., Herholz, K., Yousry, T.A., 2003. Inferior central sulcus: variations of anatomy and function on the example of the motor tongue area. NeuroImage 20, 601–610.
Fink, G.R., Frackowiak, R.S., Pietrzyk, U., Passingham, R.E., 1997. Multiple nonprimary motor areas in the human cortex. J. Neurophysiol. 77, 2164–2174.
Foltys, H., Meister, I.G., Weidemann, J., Sparing, R., Thron, A., Willmes, K., Topper, R., Hallett, M., Boroojerdi, B., 2003. Power grip disinhibits the ipsilateral sensorimotor cortex: a TMS and fMRI study. NeuroImage 19, 332–340.
Fontaine, D., Capelle, L., Duffau, H., 2002. Somatotopy of the supplementary motor area: evidence from correlation of the extent of surgical resection with the clinical patterns of deficit. Neurosurgery 50, 297–303 (discussion 303–295).
Fox, P.T., Parsons, L.M., Lancaster, J.L., 1998. Beyond the single study: function/location metanalysis in cognitive neuroimaging. Curr. Opin. Neurobiol. 8, 178–187.
Fox, P.T., Huang, A., Parsons, L.M., Xiong, J.H., Zamarippa, F., Rainey, L., Lancaster, J.L., 2001. Location-probability profiles for the mouth region of human primary motor-sensory cortex: model and validation. NeuroImage 13, 196–209.
Friston, K.J., 1997. Testing for anatomically specified regional effects. Hum. Brain Mapp. 5, 133–136.
Frutiger, S.A., Strother, S.C., Anderson, J.R., Sidtis, J.J., Arnold, J.B., Rottenberg, D.A., 2000. Multivariate predictive relationship between kinematic and functional activation patterns in a PET study of visuomotor learning. NeuroImage 12, 515–527.
Geyer, S., Schleicher, A., Zilles, K., 1997. The somatosensory cortex of human: cytoarchitecture and regional distributions of receptor-binding sites. NeuroImage 6, 27–45.
Geyer, S., Matelli, M., Luppino, G., Zilles, K., 2000. Functional neuroanatomy of the primate isocortical motor system. Anat. Embryol. (Berl.) 202, 443–474.
Geyer, S., Schormann, T., Mohlberg, H., Zilles, K., 2000. Areas 3a, 3b, and 1 of human primary somatosensory cortex: Part 2. Spatial normalization to standard anatomical space. NeuroImage 11, 684–696.
Ghilardi, M., Ghez, C., Dhawan, V., Moeller, J., Mentis, M., Nakamura, T., Antonini, A., Eidelberg, D., 2000. Patterns of regional brain activation associated with different forms of motor learning. Brain Res. 871, 127–145.
Grafton, S.T., Hazeltine, E., Ivry, R.B., 2002. Motor sequence learning with the nondominant left hand. A PET functional imaging study. Exp. Brain Res. 146, 369–378.
Grefkes, C., Geyer, S., Schormann, T., Roland, P., Zilles, K., 2001. Human somatosensory area 2 observer-independent cytoarchitectonic mapping, interindividual variability, and population map. NeuroImage 14, 617–631.
Grezes, J., Armony, J.L., Rowe, J., Passingham, R.E., 2003a. Activations related to "mirror" and "canonical" neurones in the human brain: an fMRI study. NeuroImage 18, 928–937.
Grezes, J., Tucker, M., Armony, J., Ellis, R., Passingham, R.E., 2003b. Objects automatically potentiate action: an fMRI study of implicit processing. Eur. J. Neurosci. 17, 2735–2740.
Gruber, O., von Cramon, D.Y., 2003. The functional neuroanatomy of human working memory revisited. Evidence from 3-T fMRI studies using classical domain-specific interference tasks. NeuroImage 19, 797–809.
Hamzei, F., Dettmers, C., Rijntjes, M., Glauche, V., Kiebel, S., Weber, B., Weiller, C., 2002a. Visuomotor control within a distributed parieto-frontal network. Exp. Brain Res. 146, 273–281.
Hamzei, F., Dettmers, C., Rzanny, R., Liepert, J., Buchel, C., Weiller, C., 2002b. Reduction of excitability ("inhibition") in the ipsilateral primary motor cortex is mirrored by fMRI signal decreases. NeuroImage 17, 490–496.
Haslinger, B., Erhard, P., Weilke, F., Ceballos-Baumann, A.O., Bartenstein, P., Grafin von Einsiedel, H., Schwaiger, M., Conrad, B., Boecker, H., 2002. The role of lateral premotor–cerebellar–parietal circuits in motor sequence control: a parametric fMRI study. Cogn. Brain Res. 13, 159–168.
He, S.Q., Dum, R.P., Strick, P.L., 1993. Topographic organization of corticospinal projections from the frontal lobe: motor areas on the lateral surface of the hemisphere. J. Neurosci. 13, 952–980.
Hernandez, A.E., Dapretto, M., Mazziotta, J., Bookheimer, S., 2001. Language switching and language representation in Spanish–English bilinguals: an fMRI study. NeuroImage 14, 510–520.
Holmes, A.P., Blair, R.C., Watson, J.D., Ford, I., 1996. Nonparametric analysis of statistic images from functional mapping experiments. J. Cereb. Blood Flow Metab. 16, 7–22.
Horwitz, B., Deiber, M.P., Ibanez, V., Sadato, N., Hallett, M., 2000. Correlations between reaction time and cerebral blood flow during motor preparation. NeuroImage 12, 434–441.
Indovina, I., Sanes, J.N., 2001a. Combined visual attention and finger movement effects on human brain representations. Exp. Brain Res. 140, 265–279.
Indovina, I., Sanes, J.N., 2001b. On somatotopic representation centers for finger movements in human primary motor cortex and supplementary motor area. NeuroImage 13, 1027–1034.
Ino, T., Asada, T., Ito, J., Kimura, T., Fukuyama, H., 2003. Parieto-frontal networks for clock drawing revealed with fMRI. Neurosci. Res. 45, 71–77.
Inoue, K., Kawashima, R., Satoh, K., Kinomura, S., Goto, R., Koyama, M., Sugiura, M., Ito, M., Fukuda, H., 1998. PET study of pointing with visual feedback of moving hands. J. Neurophysiol. 79, 117–125.
Inoue, K., Kawashima, R., Satoh, K., Kinomura, S., Sugiura, M., Goto, R., Ito, M., Fukuda, H., 2000. A PET study of visuomotor learning under optical rotation. NeuroImage 11, 505–516.
Jancke, L., Himmelbach, M., Shah, N.J., Zilles, K., 2000a. The effect of switching between sequential and repetitive movements on cortical activation. NeuroImage 12, 528–537.
Jancke, L., Loose, R., Lutz, K., Specht, K., Shah, N.J., 2000b. Cortical activations during paced finger-tapping applying visual and auditory pacing stimuli. Cogn. Brain Res. 10, 51–66.
Jantzen, K.J., Steinberg, F.L., Kelso, J.A., 2002. Practice-dependent modulation of neural activity during human sensorimotor coordination: a functional Magnetic Resonance Imaging study. Neurosci. Lett. 332, 205–209.
Jenkins, I.H., Passingham, R.E., Brooks, D.J., 1997. The effect of movement frequency on cerebral activation: a positron emission tomography study. J. Neurol. Sci. 151, 195–205.

Jenkins, I.H., Jahanshahi, M., Jueptner, M., Passingham, R.E., Brooks, D.J., 2000. Self-initiated versus externally triggered movements: II. The effect of movement predictability on regional cerebral blood flow. Brain 123.

Johannsen, P., Christensen, L.O., Sinkjaer, T., Nielsen, J.B., 2001. Cerebral functional anatomy of voluntary contractions of ankle muscles in man. J. Physiol. 535, 397–406.

Johansen-Berg, H., Matthews, P.M., 2002. Attention to movement modulates activity in sensori-motor areas, including primary motor cortex. Exp. Brain Res. 142, 13–24.

Johansen-Berg, H., Behrens, T.E., Robson, M.D., Drobnjak, I., Rushworth, M.F., Brady, J.M., Smith, S.M., Higham, D.J., Matthews, P.M., 2004. Changes in connectivity profiles define functionally distinct regions in human medial frontal cortex. Proc. Natl. Acad. Sci. U. S. A. 101, 13335–13340.

Johnson, S.H., Rotte, M., Grafton, S.T., Hinrichs, H., Gazzaniga, M.S., Heinze, H.J., 2002. Selective activation of a parietofrontal circuit during implicitly imagined prehension. NeuroImage 17, 1693–1704.

Joliot, M., Papathanassiou, D., Mellet, E., Quinton, O., Mazoyer, N., Courtheoux, P., Mazoyer, B., 1999. FMRI and PET of self-paced finger movement: comparison of intersubject stereotaxic averaged data. NeuroImage 10, 430–447.

Kang, A.M., Constable, R.T., Gore, J.C., Avrutin, S., 1999. An event-related fMRI study of implicit phrase-level syntactic and semantic processing. NeuroImage 10, 555–561.

Kawashima, R., Okuda, J., Umetsu, A., Sugiura, M., Inoue, K., Suzuki, K., Tabuchi, M., Tsukiura, T., Narayan, S.L., Nagasaka, T., Yanagawa, I., Fujii, T., Takahashi, S., Fukuda, H., Yamadori, A., 2000. Human cerebellum plays an important role in memory-timed finger movement: an fMRI study. J. Neurophysiol. 83, 1079–1087.

Kawashima, R., Tajima, N., Yoshida, H., Okita, K., Sasaki, T., Schormann, T., Ogawa, A., Fukuda, H., Zilles, K., 2000. The effect of verbal feedback on motor learning — A PET study. Positron emission tomography. NeuroImage 12, 698–706.

Kinoshita, H., Oku, N., Hashikawa, K., Nishimura, T., 2000. Functional brain areas used for the lifting of objects using a precision grip: a PET study. Brain Res. 857, 119–130.

Kobayashi, M., Hutchinson, S., Schlaug, G., Pascual-Leone, A., 2003. Ipsilateral motor cortex activation on functional magnetic resonance imaging during unilateral hand movements is related to interhemispheric interactions. NeuroImage 20, 2259–2270.

Koechlin, E., Corrado, G., Pietrini, P., Grafman, J., 2000. Dissociating the role of the medial and lateral anterior prefrontal cortex in human planning. Proc. Natl. Acad. Sci. 97, 7651–7656.

Koski, L., Wohlschlager, A., Bekkering, H., Woods, R.P., Dubeau, M.C., Mazziotta, J.C., Iacoboni, M., 2002. Modulation of motor and premotor activity during imitation of target-directed actions. Cereb. Cortex 12, 847–855.

Krams, M., Rushworth, M.F., Deiber, M.P., Frackowiak, R.S., Passingham, R.E., 1998. The preparation, execution and suppression of copied movements in the human brain. Exp. Brain Res. 120, 386–398.

Kuhtz-Buschbeck, J.P., Ehrsson, H.H., Forssberg, H., 2001. Human brain activity in the control of fine static precision grip forces: an fMRI study. Eur. J. Neurosci. 14, 382–390.

Lacquaniti, F., Perani, D., Guigon, E., Bettinardi, V., Carrozzo, M., Grassi, F., Rossetti, Y., Fazio, F., 1997. Visuomotor transformations for reaching to memorized targets: a PET study. NeuroImage 5, 129–146.

Lafleur, M.F., Jackson, P.L., Malouin, F., Richards, C.L., Evans, A.C., Doyon, J., 2002. Motor learning produces parallel dynamic functional changes during the execution and imagination of sequential foot movements. NeuroImage 16, 142–157.

Lamm, C., Windischberger, C., Leodolter, U., Moser, E., Bauer, H., 2001. Evidence for premotor cortex activity during dynamic visuospatial imagery from single-trial functional magnetic resonance imaging and event-related slow cortical potentials. NeuroImage 14, 268–283.

Lazar, N.A., Luna, B., Sweeney, J.A., Eddy, W.F., 2002. Combining brains: a survey of methods for statistical pooling of information. NeuroImage 16, 538–550.

Lehericy, S., Ducros, M., Krainik, A., Francois, C., Van de Moortele, P.F., Ugurbil, K., Kim, D.S., 2004. 3-D diffusion tensor axonal tracking shows distinct SMA and pre-SMA projections to the human striatum. Cereb. Cortex 14, 1302–1309.

Leube, D.T., Knoblich, G., Erb, M., Grodd, W., Bartels, M., Kircher, T.T., 2003. The neural correlates of perceiving one's own movements. NeuroImage 20, 2084–2090.

Li, G., Liu, H.L., Cheung, R.T., Hung, Y.C., Wong, K.K., Shen, G.G., Ma, Q.Y., Yang, E.S., 2003. An fMRI study comparing brain activation between word generation and electrical stimulation of language-implicated acupoints. Hum. Brain Mapp. 18, 233–238.

Liddle, P.F., Kiehl, K.A., Smith, A.M., 2001. Event-related fMRI study of response inhibition. Hum. Brain Mapp. 12, 100–109.

Lotze, M., Seggewies, G., Erb, M., Grodd, W., Birbaumer, N., 2000. The representation of articulation in the primary sensorimotor cortex. NeuroReport 11, 2985–2989.

Lotze, M., Braun, C., Birbaumer, N., Anders, S., Cohen, L.G., 2003. Motor learning elicited by voluntary drive. Brain 126, 866–872.

Luppino, G., Rizzolatti, G., 2000. The organization of the frontal motor cortex. News Physiol. Sci. 15, 219–224.

Luppino, G., Matelli, M., Camarda, R.M., Gallese, V., Rizzolatti, G., 1991. Multiple representations of body movements in mesial area 6 and the adjacent cingulate cortex: an intracortical microstimulation study in the macaque monkey. J. Comp. Neurol. 311, 463–482.

Maguire, R.P., Broerse, A., de Jong, B.M., Cornelissen, F.W., Meiners, L.C., Leenders, K.L., den Boer, J.A., 2003. Evidence of enhancement of spatial attention during inhibition of a visuo-motor response. NeuroImage 20, 1339–1345.

Malouin, F., Richards, C.L., Jackson, P.L., Dumas, F., Doyon, J., 2003. Brain activations during motor imagery of locomotor-related tasks: a PET study. Hum. Brain Mapp. 19, 47–62.

Manthey, S., Schubotz, R.I., von Cramon, D.Y., 2003. Premotor cortex in observing erroneous action: an fMRI study. Brain Res. Cogn. Brain Res. 15, 296–307.

Martin, R.E., Goodyear, B.G., Gati, J.S., Menon, R.S., 2001. Cerebral cortical representation of automatic and volitional swallowing in humans. J. Neurophysiol. 85, 938–950.

Matelli, M., Luppino, G., Rizzolatti, G., 1985. Patterns of cytochrome oxidase activity in the frontal agranular cortex of the macaque monkey. Behav. Brain Res. 18, 125–136.

Matelli, M., Luppino, G., Rizzolatti, G., 1991. Architecture of superior and mesial area 6 and the adjacent cingulate cortex in the macaque monkey. J. Comp. Neurol. 311, 445–462.

Matsuo, K., Kato, C., Okada, T., Moriya, T., Glover, G.H., Nakai, T., 2003. Finger movements lighten neural loads in the recognition of ideographic characters. Brain Res. Cogn. Brain Res. 17, 263–272.

Matsuzaka, Y., Aizawa, H., Tanji, J., 1992. A motor area rostral to the supplementary motor area (presupplementary motor area) in the monkey: neuronal activity during a learned motor task. J. Neurophysiol. 68, 653–662.

Mattay, V.S., Callicott, J.H., Bertolino, A., Santha, A.K., Van Horn, J.D., Tallent, K.A., Frank, J.A., Weinberger, D.R., 1998. Hemispheric control of motor function: a whole brain echo planar fMRI study. Psychiatry Res.: Neuroimaging Sect. 83, 7–22.

Mayer, A.R., Zimbelman, J.L., Watanabe, Y., Rao, S.M., 2001. Somatotopic organization of the medial wall of the cerebral hemispheres: a 3 Tesla fMRI study. NeuroReport 12, 3811–3814.

Mayville, J.M., Jantzen, K.J., Fuchs, A., Steinberg, F.L., Kelso, J.A., 2002. Cortical and subcortical networks underlying syncopated and synchronized coordination revealed using fMRI. Functional magnetic resonance imaging. Hum. Brain Mapp. 17, 214–229.

Mitz, A.R., Wise, S.P., 1987. The somatotopic organization of the supplementary motor area: intracortical microstimulation mapping. J. Neurosci. 7, 1010–1021.

Moore, C.I., Stern, C.E., Corkin, S., Fischl, B., Gray, A.C., Rosen, B.R., Dale, A.M., 2000. Segregation of somatosensory activation in the human rolandic cortex using fMRI. J. Neurophysiol. 84, 558–569.

Muley, S.A., Strother, S.C., Ashe, J., Frutiger, S.A., Anderson, J.R., Sidtis, J.J., Rottenberg, D.A., 2001. Effects of changes in experimental design on PET studies of isometric force. NeuroImage 13, 185–195.

Muller, R.A., Kleinhans, N., Pierce, K., Kemmotsu, N., Courchesne, E., 2002. Functional MRI of motor sequence acquisition: effects of learning stage and performance. Cogn. Brain Res. 14, 277–293.

Nakai, T., Kato, C., Glover, G.H., Toma, K., Moriya, T., Matsuo, K., 2003. A functional magnetic resonance imaging study of internal modulation of an external visual cue for motor execution. Brain Res. 968, 238–247.

Nichols, T.E., Holmes, A.P., 2002. Nonparametric permutation tests for functional neuroimaging: a primer with examples. Hum. Brain Mapp. 15, 1–25.

Nowak, M., Olsen, K.S., Law, I., Holm, S., Paulson, O.B., Secher, N.H., 1999. Command-related distribution of regional cerebral blood flow during attempted handgrip. J. Appl. Physiol. 86, 819–824.

Nyberg, L., Petersson, K.M., Nilsson, L.G., Sandblom, J., Aberg, C., Ingvar, M., 2001. Reactivation of motor brain areas during explicit memory for actions. NeuroImage 14, 521–528.

Oishi, K., Toma, K., Matsuo, K., Nakai, T., Chihara, K., Fukuyama, H., 2003. Cortical motor areas in plantar response: an event-related functional magnetic resonance imaging study in normal subjects. Neurosci. Lett. 345, 17–20.

Palmer, E.D., Rosen, H.J., Ojemann, J.G., Buckner, R.L., Kelley, W.M., Petersen, S.E., 2001. An event-related fMRI study of overt and covert word stem completion. NeuroImage 14, 182–193.

Paus, T., 1996. Location and function of the human frontal eye-field: a selective review. Neuropsychologia 34, 475–483.

Paus, T., Tomaiuolo, F., Otaky, N., MacDonald, D., Petrides, M., Atlas, J., Morris, R., Evans, A.C., 1996. Human cingulate and paracingulate sulci: pattern, variability, asymmetry, and probabilistic map. Cereb. Cortex 6, 207–214.

Penfield, W., Welch, K., 1951. The supplementary motor area of the cerebral cortex; a clinical and experimental study. AMA Arch. Neurol. Psychiatry 66, 289–317.

Penhune, V.B., Doyon, J., 2002. Dynamic cortical and subcortical networks in learning and delayed recall of timed motor sequences. J. Neurosci. 22, 1397–1406.

Petit, L., Dubois, S., Tzourio, N., Dejardin, S., Crivello, F., Michel, C., Etard, O., Denise, P., Roucoux, A., Mazoyer, B., 1999. PET study of the human foveal fixation system. Hum. Brain Mapp. 8, 28–43.

Picard, N., Strick, P.L., 1996. Motor areas of the medial wall: a review of their location and functional activation. Cereb. Cortex 6, 342–353.

Picard, N., Strick, P.L., 2001. Imaging the premotor areas. Curr. Opin. Neurobiol. 11, 663–672.

Rademacher, J., Caviness, V.S. Jr., Steinmetz, H., Galaburda, A.M., 1993. Topographical variation of the human primary cortices: implications for neuroimaging, brain mapping, and neurobiology. Cereb. Cortex 3, 313–329.

Rademacher, J., Morosan, P., Schormann, T., Schleicher, A., Werner, C., Freund, H.J., Zilles, K., 2001a. Probabilistic mapping and volume measurement of human primary auditory cortex. NeuroImage 13, 669–683.

Rademacher, J., Burgel, U., Geyer, S., Schormann, T., Schleicher, A., Freund, H.J., Zilles, K., 2001b. Variability and asymmetry in the human precentral motor system. A cytoarchitectonic and myeloarchitectonic brain mapping study. Brain 124, 2232–2258.

Rao, S.M., Harrington, D.L., Haaland, K.Y., Bobholz, J.A., Cox, R.W., Binder, J.R., 1997. Distributed neural systems underlying the timing of movements. J. Neurosci. 17, 5528–5535.

Rauch, S.L., Whalen, P.J., Savage, C.R., Curran, T., Kendrick, A., Brown, H.D., Bush, G., Breiter, H.C., Rosen, B.R., 1997. Striatal recruitment during an implicit sequence learning task as measured by functional magnetic resonance imaging. Hum. Brain Mapp. 5, 124–132.

Riecker, A., Wildgruber, D., Dogil, G., Grodd, W., Ackermann, H., 2002. Hemispheric lateralization effects of rhythm implementation during syllable repetitions: an fMRI study. NeuroImage 16, 169–176.

Riecker, A., Wildgruber, D., Mathiak, K., Grodd, W., Ackermann, H., 2003. Parametric analysis of rate-dependent hemodynamic response functions of cortical and subcortical brain structures during auditorily cued finger tapping: a fMRI study. NeuroImage 18, 731–739.

Rizzolatti, G., Luppino, G., 2001. The cortical motor system. Neuron 31, 889–901.

Rizzolatti, G., Luppino, G., Matelli, M., 1998. The organization of the cortical motor system: new concepts. Electroencephalogr. Clin. Neurophysiol. 106, 283–296.

Rizzolatti, G., Fogassi, L., Gallese, V., 2002. Motor and cognitive functions of the ventral premotor cortex. Curr. Opin. Neurobiol. 12, 149–154.

Roland, P.E., Zilles, K., 1996. Functions and structures of the motor cortices in humans. Curr. Opin. Neurobiol. 6, 773–781.

Roland, P.E., Zilles, K., 1998. Structural divisions and functional fields in the human cerebral cortex. Brain Res. Brain Res. Rev. 26, 87–105.

Rosano, C., Krisky, C.M., Welling, J.S., Eddy, W.F., Luna, B., Thulborn, K.R., Sweeney, J.A., 2002. Pursuit and saccadic eye movement subregions in human frontal eye field: a high-resolution fMRI investigation. Cereb. Cortex 12, 107–115.

Rosner, B., 2000. Fundamentals of Biostatistics, 5th Edition Duxbury Tomson Learning.

Rotte, M., Kanowski, M., Heinze, H.J., 2002. Functional magnetic resonance imaging for the evaluation of the motor system: primary and secondary brain areas in different motor tasks. Stereotact. Funct. Neurosurg. 78, 3–16.

Rowe, J., Stephan, K.E., Friston, K., Frackowiak, R., Lees, A., Passingham, R., 2002. Attention to action in Parkinson's disease: impaired effective connectivity among frontal cortical regions. Brain 125, 276–289.

Russo, G.S., Backus, D.A., Ye, S., Crutcher, M.D., 2002. Neural activity in monkey dorsal and ventral cingulate motor areas: comparison with the supplementary motor area. J. Neurophysiol. 88, 2612–2629.

Sadato, N., Yonekura, Y., Waki, A., Yamada, H., Ishii, Y., 1997. Role of the supplementary motor area and the right premotor cortex in the coordination of bimanual finger movements. J. Neurosci. 17, 9667–9674.

Saito, D.N., Okada, T., Morita, Y., Yonekura, Y., Sadato, N., 2003. Tactile–visual cross-modal shape matching: a functional MRI study. Brain Res. Cogn. Brain Res. 17, 14–25.

Sakai, K., Hikosaka, O., Miyauchi, S., Takino, R., Tamada, T., Iwata, N.K., Nielsen, M., 1999. Neural representation of a rhythm depends on its interval ratio. J. Neurosci. 19, 10074–10081.

Sakai, K., Hikosaka, O., Takino, R., Miyauchi, S., Nielsen, M., Tamada, T., 2000. What and when: parallel and convergent processing in motor control. J. Neurosci. 20, 2691–2700.

Schubotz, R.I., von Cramon, D.Y., 2001. Interval and ordinal properties of sequences are associated with distinct premotor areas. Cereb. Cortex 11, 210–222.

Schubotz, R.I., von Cramon, D.Y., 2002a. A blueprint for target motion: fMRI reveals perceived sequential complexity to modulate premotor cortex. NeuroImage 16, 920–935.

Schubotz, R.I., von Cramon, D., 2002b. Dynamic patterns make the premotor cortex interested in objects: influence of stimulus and task revealed by fMRI. Cogn. Brain Res. 14, 357–369.

Schubotz, R.I., von Cramon, D.Y., 2003. Functional–anatomical concepts of human premotor cortex: evidence from fMRI and PET studies. NeuroImage 20 (Suppl. 1), S120–S131.

Schumacher, E.H., Lauber, E., Awh, E., Jonides, J., Smith, E.E., Koeppe, R.A., 1996. PET evidence for an amodal verbal working memory system. NeuroImage 3, 79–88.

Siebner, H.R., Limmer, C., Peinemann, A., Bartenstein, P., Drzezga, A., Conrad, B., 2001. Brain correlates of fast and slow handwriting in humans: a PET-performance correlation analysis. Eur. J. Neurosci. 14, 726–736.

Simon, S.R., Meunier, M., Piettre, L., Berardi, A.M., Segebarth, C.M., Boussaoud, D., 2002. Spatial attention and memory versus motor preparation: premotor cortex involvement as revealed by fMRI. J. Neurophysiol. 88, 2047–2057.

Siok, W.T., Jin, Z., Fletcher, P., Tan, L.H., 2003. Distinct brain regions associated with syllable and phoneme. Hum. Brain Mapp. 18, 201–207.

Solodkin, A., Hlustik, P., Noll, D.C., Small, S.L., 2001. Lateralization of

motor circuits and handedness during finger movements. Eur. J. Neurosci. 8, 425–434.
Staines, W.R., Graham, S.J., Black, S.E., McIlroy, W.E., 2002. Task-relevant modulation of contralateral and ipsilateral primary somatosensory cortex and the role of a prefrontal-cortical sensory gating system. NeuroImage 15, 190–199.
Stephan, K.M., Thaut, M.H., Wunderlich, G., Schicks, W., Tian, B., Tellmann, L., Schmitz, T., Herzog, H., McIntosh, G.C., Seitz, R.J., Homberg, V., 2002. Conscious and subconscious sensorimotor synchronization-prefrontal cortex and the influence of awareness. NeuroImage 15, 345–352.
Stippich, C., Ochmann, H., Sartor, K., 2002. Somatotopic mapping of the human primary sensorimotor cortex during motor imagery and motor execution by functional magnetic resonance imaging. Neurosci. Lett. 331, 50–54.
Stoeckel, M.C., Weder, B., Binkofski, F., Buccino, G., Shah, N.J., Seitz, R.J., 2003. A fronto-parietal circuit for tactile object discrimination: an event-related fMRI study. NeuroImage 19, 1103–1114.
Sugio, T., Ogawa, K., Inui, T., 2003. Neural correlates of semantic effects on grasping familiar objects. NeuroReport 14, 2297–2301.
Talairach, J., Tournoux, P., 1988. Co-planar Stereotaxic Atlas of the Human Brain: 3-Dimensional Proportional System: An Approach to Cerebral Imaging. Thieme Medical Publishers, Inc, New York, NY.
Tan, L.H., Spinks, J.A., Feng, C.M., Siok, W.T., Perfetti, C.A., Xiong, J., Fox, P.T., Gao, J.H., 2003. Neural systems of second language reading are shaped by native language. Hum. Brain Mapp. 18, 158–166.
Toma, K., Ozawa, M., Matsuo, K., Nakai, T., Fukuyama, H., Sato, S., 2003. The role of the human supplementary motor area in reactive motor operation. Neurosci. Lett. 344, 177–180.
Toni, I., Passingham, R.E., 1999. Prefrontal-basal ganglia pathways are involved in the learning of arbitrary visuomotor associations: a PET study. Exp. Brain Res. 127, 19–32.
Toni, I., Krams, M., Turner, R., Passingham, R.E., 1998. The time course of changes during motor sequence learning: a whole-brain fMRI study. NeuroImage 8, 50–61.
Toni, I., Ramnani, N., Josephs, O., Ashburne, J., Passingham, R.E., 2001a. Learning arbitrary visuomotor associations: temporal dynamic of brain activity. NeuroImage 14, 1048–1057.
Toni, I., Rushworth, M.F., Passingham, R.E., 2001b. Neural correlates of visuomotor associations. Spatial rules compared with arbitrary rules. Exp. Brain Res. 141, 359–369.
Toni, I., Shah, N.J., Fink, G.R., Thoenissen, D., Passingham, R.E., Zilles, K., 2002. Multiple movement representations in the human brain: an event-related fMRI study. J. Cogn. Neurosci. 14, 769–784.
Tracy, J.I., Faro, S.S., Mohammed, F.B., Pinus, A.B., Madi, S.M., Laskas, J.W., 2001. Cerebellar mediation of the complexity of bimanual compared to unimanual movements. Neurology 57, 1862–1869.
Tracy, J., Flanders, A., Madi, S., Laskas, J., Stoddard, E., Pyrros, A., Natale, P., DelVecchio, N., 2003. Regional brain activation associated with different performance patterns during learning of a complex motor skill. Cereb. Cortex 13, 904–910.
Turkeltaub, P.E., Eden, G.F., Jones, K.M., Zeffiro, T.A., 2002. Meta-analysis of the functional neuroanatomy of single-word reading: method and validation. NeuroImage 16, 765–780.
Turner, R.S., Desmurget, M., Grethe, J., Crutcher, M.D., Grafton, S.T., 1998. Motor subcircuits mediating the control of movement extent and speed. J. Neurophysiol. 80, 2162–2176.
Tzourio, N., Crivello, F., Mellet, E., Nkanga-Ngila, B., Mazoyer, B., 1998. Functional anatomy of dominance for speech comprehension in left handers vs. right handers. NeuroImage 8, 1–16.
Ullen, F., Forssberg, H., Ehrsson, H.H., 2003. Neural networks for the coordination of the hands in time. J. Neurophysiol. 89, 1126–1135.
Ullsperger, M., von Cramon, D.Y., 2001. Subprocesses of performance monitoring: a dissociation of error processing and response competition revealed by event-related fMRI and ERPs. NeuroImage 14, 1387–1401.
Urasaki, E., Uematsu, S., Gordon, B., Lesser, R.P., 1994. Cortical tongue area studied by chronically implanted subdural electrodes—With special reference to parietal motor and frontal sensory responses. Brain 117 (Pt. 1), 117–132.
Vaillancourt, D.E., Thulborn, K.R., Corcos, D.M., 2003. Neural basis for the processes that underlie visually guided and internally guided force control in humans. J. Neurophysiol. 90, 3330–3340.
Vaillancourt, D.E., Mayka, M.A., Corcos, D.M., 2006. Intermittent visuomotor processing in the human cerebellum, parietal cortex, and premotor cortex. J. Neurophysiol. 95, 922–931.
van Mier, H., Tempel, L.W., Perlmutter, J.S., Raichle, M.E., Petersen, S.E., 1998. Changes in brain activity during motor learning measured with PET: effects of hand of performance and practice. J. Neurophysiol. 80, 2177–2199.
Viviani, P., Perani, D., Grassi, F., Bettinardi, V., Fazio, F., 1998. Hemispheric asymmetries and bimanual asynchrony in left- and right-handers. Exp. Brain Res. 120, 531–536.
Vogt, B.A., Nimchinsky, E.A., Vogt, L.J., Hof, P.R., 1995. Human cingulate cortex: surface features, flat maps, and cytoarchitecture. J. Comp. Neurol. 359, 490–506.
Vorobiev, V., Govoni, P., Rizzolatti, G., Matelli, M., Luppino, G., 1998. Parcellation of human mesial area 6 cytoarchitectonic evidence for three separate areas. Eur, J., Neurosci 10, 2199–2203.
Wang, Y., Shima, K., Isoda, M., Sawamura, H., Tanji, J., 2002. Spatial distribution and density of prefrontal cortical cells projecting to three sectors of the premotor cortex. NeuroReport 13, 1341–1344.
Watanabe, J., Sugiura, M., Sato, K., Sato, Y., Maeda, Y., Matsuem, Y., Fukuda, H., Kawashima, R., 2002. The human prefrontal and parietal association cortices are involved in NO-GO performances: an event-related fMRI study. NeuroImage 17, 1207–1216.
Weiss, P.H., Marshall, J.C., Zilles, K., Fink, G.R., 2003. Are action and perception in near and far space additive or interactive factors? NeuroImage 18, 837–846.
White, L.E., Andrews, T.J., Hulette, C., Richards, A., Groelle, M., Paydarfar, J., Purves, D., 1997. Structure of the human sensorimotor system. I: Morphology and cytoarchitecture of the central sulcus. Cereb. Cortex 7, 18–30.
Wildgruber, D., Ackermann, H., Grodd, W., 2001. Differential contributions of motor cortex, basal ganglia, and cerebellum to speech motor control: effects of syllable repetition rate evaluated by fMRI. NeuroImage 13, 101–109.
Winstein, C.J., Grafton, S.T., Pohl, P.S., 1997. Motor task difficulty and brain activity: investigation of goal-directed reciprocal aiming using positron emission tomography. J. Neurophysiol. 77, 1581–1594.
Winterer, G., Adams, C.M., Jones, D.W., Knutson, B., 2002. Volition to action—An event-related fMRI study. NeuroImage 17, 851–858.
Woods, R.P., 1996. Modeling for intergroup comparisons of imaging data. NeuroImage 4, S84–S94.
Woolsey, C.N., Settlage, P.H., Meyer, D.R., Sencer, W., Pinto Hamuy, T., Travis, A.M., 1952. Patterns of localization in precentral and "supplementary" motor areas and their relation to the concept of a premotor area. Res. Publ. Assoc. Res. Nerv. Ment. Dis. 30, 238–264.
Woolsey, C.N., Erickson, T.C., Gilson, W.E., 1979. Localization in somatic sensory and motor areas of human cerebral cortex as determined by direct recording of evoked potentials and electrical stimulation. J. Neurosurg. 51, 476–506.
Worsley, K.J., Marrett, S., Neelin, P., Vandal, A.C., Fristron, K.J., Evans, A.C., 1996. A unified statistical approach for determining significant signals in images of cerebral activation. Hum. Brain Mapp. 4, 58–73.
Yoo, S.S., Freeman, D.K., McCarthy, J.J. III, Jolesz, F.A., 2003. Neural substrates of tactile imagery: a functional MRI study. NeuroReport 14, 581–585.
Yousry, T.A., Schmid, U.D., Alkadhi, H., Schmidt, D., Peraud, A., Buettner, A., Winkler, P., 1997. Localization of the motor hand area to a knob on the precentral gyrus. A new landmark. Brain 120 (Pt. 1), 141–157.
Zhou, S.Y., Suzuki, M., Hagino, H., Takahashi, T., Kawasaki, Y., Matsui, M., Seto, H., Kurachi, M., 2005. Volumetric analysis of sulci/gyri-defined in vivo frontal lobe regions in schizophrenia: Precentral gyrus, cingulate gyrus, and prefrontal region. Psychiatry Res. 139, 127–139.